

Tectono-magmatic response to major convergence changes in the North Patagonian suprasubduction system; the Paleogene subduction–transcurrent plate margin transition

Eugenio Aragón ^{a,b,k,*}, Fernando D'Eramo ^c, Antonio Castro ^d, Lucio Pinotti ^c, Daniele Brunelli ^{e,f}, Osvaldo Rabbia ^g, Giorgio Rivalenti ^e, Ricardo Varela ^{a,b}, Wim Spakman ^h, Manuel Demartis ^c, Claudia E. Cavarozzi ^{a,b}, Yolanda E. Aguilera ^{b,i}, Maurizio Mazzucchelli ^e, Alejandro Ribot ^{b,j}

^a Centro de Investigaciones Geológicas (UNLP-CONICET), 1 No 644. (1900) La Plata, Buenos Aires, Argentina

^b Facultad de Ciencias Naturales y Museo, Universidad Nacional de la Plata, 122 y 60, s/n. (1900), La Plata, Buenos Aires, Argentina

^c Departamento de Geología, Universidad Nacional de Río Cuarto, (UNRC-CONICET), Ruta 36 km 601, Río Cuarto, Córdoba, Argentina

^d Departamento de Geología, Universidad de Huelva, 21071 Huelva, Spain

^e Dipartimento di Scienze Della Terra, Università degli Studi di Modena, Piazzale S. Eufemia, 19, I-41100 Modena, Italy

^f Istituto di Scienze Marine, CNR, Via Gobetti 101, 40129, Bologna, Italy

^g Instituto de Geología Económica Aplicada, Universidad de Concepción, Chile

^h Vening Meinesz Research School of Geodynamics, Faculty of Earth Sciences, Utrecht University, Netherlands

ⁱ Dirección de Aplicación de Imágenes Satelitarias (M.O.S.P.). 58 e/7 y 8, piso 2, 1900, La Plata, Buenos Aires, Argentina

^j LEMIT-CIC, 52 entre 121 y 122, 1900, La Plata, Buenos Aires, Argentina

^k Universidad Nacional de Río Negro, Isidro Lobo y Belgrano, (8332) Roca, Río Negro, Argentina

ARTICLE INFO

Article history:

Received 5 January 2010

Received in revised form 7 June 2011

Accepted 10 June 2011

Available online 21 June 2011

Keywords:

Andes

Subduction–transform transition

Transcurrent plate margin

Synextensional calc-alkaline

Tectonic inversion

Uplift

ABSTRACT

The southern and central Andes reflect significant along-strike differences of tectonic activity, including shortening, alternating flat-to-normal subduction styles and magmatism. In northern Patagonia, the subduction/supra-subduction system, fore arc, arc and back arc basins developed in an extensional setting during the Paleogene. This was accompanied by landward migration of calc-alkalic magmatism which changed to synextensional bimodal volcanism of rhyolitic ignimbrites and interbedded tholeiitic and alkalic basalts. These Paleogene events occurred during a time when the Farallon–Aluk active ridge reached the South American plate, and the Farallon plate subduction was interrupted. They represent a new tectonic regime, characterized by a transcurrent plate margin. The presence in the back arc of a rigid lithospheric block of 100,000 km² represented by the North Patagonian Massif focused the rotation of the coastal blocks. This resulted in the development of two Paleogene extensional regions to the north and south, respectively, of the Massif and replaced the former back arc. Plate rearrangement caused by the inauguration of the Nazca plate and its regime of orthogonal subduction at the beginning of the Miocene, re-established typical calc-alkaline arc magmatism at the former upper Cretaceous arc locus. Present seismic activity in the subducted plate and tomographic modeling of p-wave velocity anomalies in the upper mantle also suggest the presence of a subduction gap that lasted for most of the Paleogene in northern Patagonia.

© 2011 Elsevier B.V. All rights reserved.

1. Introduction

Local complexities and along-plate changes in the tectonic regime are characteristic features of the active continental margin of the Americas. The Andean margin in South America is a good example in which major changes can be recognized from the early Tertiary to the present. The geometry of the subducted slab along the Andean margin varies in dip from sub horizontal flat-slab segments to normal

subduction (dipping around 30°) (Barazangi and Isacks, 1979; Cahill and Isacks, 1992; Engdahl et al., 1995, 1998). Northern Patagonia is a normal subduction segment bounded to the north by northern Chile flat-slab segment (27° to 33°S), and to the south (47° to 55°S) by a shallow dip slab segment (Heintz et al., 2005).

These variations have drastic effects in the tectonic style, the evolution of sedimentary basins and the cycles of magmatism from extensional to compressional regimes. These major changes can be recognized and characterized at present by direct observation and deep geophysical surveys (Barazangi and Isacks, 1979; Bijwaard et al., 1998; Cahill and Isacks, 1992; Engdahl et al., 1995; Heintz et al., 2005; Tassara and Yáñez, 2003). However, their identification in past times requires detailed field-based studies and a careful characterization of

* Corresponding author at: Facultad de Ciencias Naturales y Museo, Universidad Nacional de la Plata, 122 y 60, s/n. (1900), La Plata, Buenos Aires, Argentina. Tel.: +54 221 4709985.

E-mail address: earagon@cig.museo.unlp.edu.ar (E. Aragón).

magmatic rocks as witnesses of past deep-seated processes. In particular, the marked along-strike differences in the late Tertiary tectonic evolution of the central and southern Andes gives an excellent opportunity to study the interplay between angle of convergence, subduction geometry and tectonic response of the overriding heterogeneous continental lithosphere.

The aim of this paper is two-fold. On one hand, we show geologic, geochemical and geophysical evidence that suggest the presence of a Paleogene subduction gap of northern Patagonia (Fig. 1A). On the other hand, we propose a new regional tectonic model to explain this

Paleogene subduction gap that is characterized by bimodal synextensional calc-alkaline, tholeiitic and alkaline volcanism at a distance of 400 km from the former arc trench.

2. Geological setting and main tectono-magmatic constraints of the northern Patagonian region

Three main geological constraints are crucial to understand the tectono-magmatic evolution of the northern Patagonian region during late Mesozoic and Tertiary times. These are (1) the North Patagonian

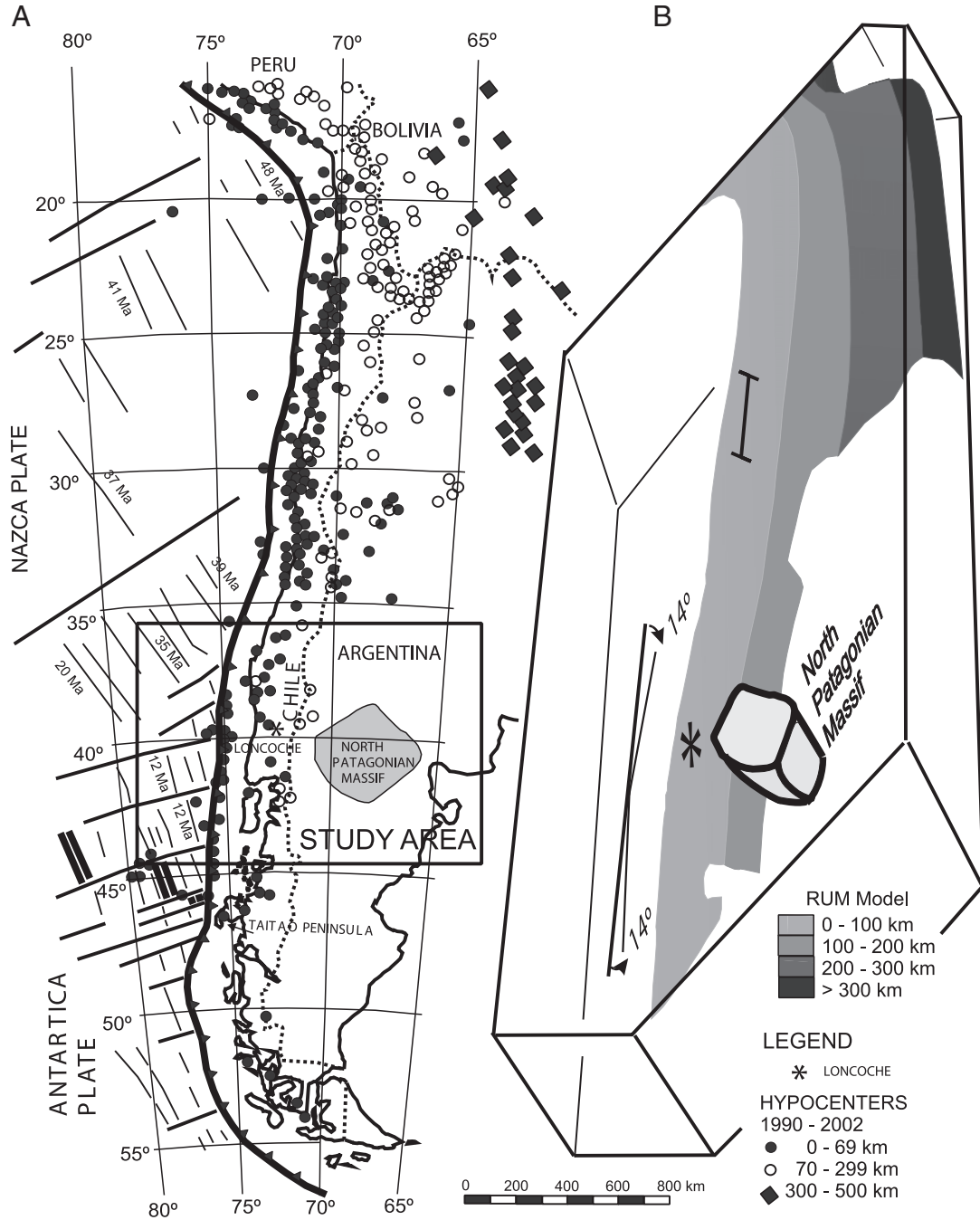


Fig. 1. (A) Seismicity and schematic geodynamic setting of the Andean Margin. Major hypocenter distribution (see legend) shows differences between southern and northern Andes. The subduction trench (barbed solid line) and the age of the oceanic plate is indicated per each accretionary segment, along with the primary morphologic structures of the oceanic crust. * indicates Loncoche area. The gray area is the North Patagonian Massif. The location at the trench of the boundary between Antarctica and Nazca plates is at the Taitao Peninsula. (B) Geometry of the subduction slab beneath South American plate modified after the Regionalized Upper Mantle model (Gudmundsson and Sambridge, 1998). The location of the North Patagonian Massif is sketched based on topographic and tomographic data. Thick brackets show flat slab segments (Gutscher et al., 2000). The symbol * shows the location of the Loncoche area interpreted as the center of the partial rotation of the northern and southern coastal blocks. Neogene clockwise coastal block rotation (to the north of Loncoche) is from Beck et al., 2000; the counter-clockwise coastal block rotation (to the south of Loncoche) is from Beck et al. (1986).

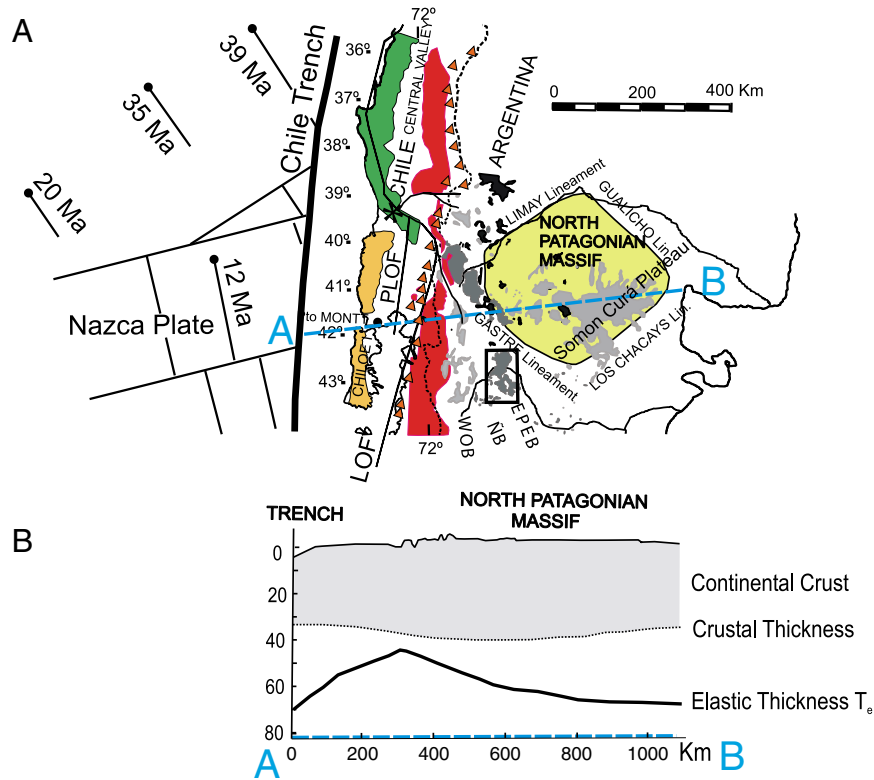
Batholith (NPB) and Cenozoic volcanic activity with respect to plate tectonic history, (2) the role of the North Patagonian Massif (NPM) in the back arc, and (3) Tertiary rotation and drift history of the coastal blocks. The most outstanding features of these three elements (Fig. 2A) are depicted here based on previously published studies. The correlation with the new geochemical (volcanism) and seismic data will be discussed later on in this paper.

2.1. The Northern Patagonian Batholith, the Cenozoic volcanic activity and the plate tectonic history

The northern segment of the Northern Patagonian Batholith (NPB; 44° S to 36° S) shows a Paleogene decrease of magmatic activity that leads to a magmatic gap from ~30 to ~15 Ma (Aragón et al., in press; Cingolani et al., 1991; González Diaz, 1982; Munizaga et al., 1988; Pankhurst et al., 1999; Rapela, 1987). The upper Miocene plutonic

rocks formed after the gap are bimodal, with predominant gabbro and leucogranite compositions, in contrast to the abundant intermediate rocks of the upper Cretaceous batholith (Rapela and Kay, 1988).

The decrease of magmatic activity (plutonic) in the NPB was accompanied by an eastward shifting of the calc-alkaline magmatic alignment (volcanic) to the position formerly occupied by the back arc region (Rapela et al., 1987) as a bimodal volcanic belt (the Eastern Paleocene–Eocene volcanic belt (EPEB) Fig. 2A). The EPEB silicic volcanism develops a large upper Paleocene–Eocene ignimbrite flare-up, interbedded with minor Eocene tholeiitic lavas (Aragón et al., 2004b) and alkalic lavas (Aragón et al., 2005). This volcanism is coeval with extension that was identified in both back arc (Cazau et al., 1989; Giacosa and Heredia 2004; Giacosa and Márquez, 1999; Mancini and Serna, 1989; Silvestro and Zubiri, 2008) and fore arc locations (Charrier et al., 2002; Jordan et al., 2001). Tectonic inversion took place in the upper Miocene (Charrier et al., 2002; Giacosa and



REFERENCES

- | | |
|-------------------------------------|--|
| 12 Ma Age of ocean floor | ■ WOB = Western Oligocene volcanic Belt |
| LOF Liquiñe Ofqui Fault | ■ EPEB = Eastern Paleocene–Eocene volcanic Belt |
| PLOF Proto Liquiñe Ofqui Fault | ■ Northpatagonian Batholith with Cretaceous and Miocene plutonic rocks |
| * Loncoche area | ■ Coast Range and transverse Range |
| ▲ Neogene volcanoes (SVZ) | ■ Peninsular Coast Range |
| ■ Neogene back arc alkaline basalts | ■ North Patagonian Massif |
| ÑB Ñirihuau basin | □ Río Chubut medio sampling locality |

Fig. 2. Geotectonic constraints of northern Patagonia. A) Selected tectono-magmatic units of northern Patagonia and South-central Chile: (1) The Chilean Coast Ranges are subdivided into (a) The Peninsular Coast Range; composed of blocks that moved northward more than 400 km. and that stand against a Transverse Range. (b) The Coast Range (sensu stricto); it consists of the metamorphic pair (Serie Oriental with Low P/T gradient, Serie Occidental with High P/T gradient) and rocks of Permian–Triassic age. (c) The Transverse Range; comprises the eastwardly bent geological units of the Coast Range s.s. The Transverse Range separates the Central Valley to the north, from an embayment influenced valley to the south. (2) The subduction related magmatic belts are shown by the North Patagonian Batholith and units constructed by Neogene arc volcanism. (3) Synextensional back-arc calc-alkalic and alkalic volcanism is indicated by the Eocene and Oligocene belts and the Somon Cura plateau lavas. (4) The North Patagonian Massif is bounded by the Gualicho, Limay, Gastre and Los Chacays lineaments. B) Profile across South American plate at North Patagonian Massif latitude ~42°S (A–B at Fig. 3A) with gravity-modeled crustal thickness and elastic thickness after Tassara and Yáñez (2003). Note the greater crustal thickness (>5 km) beneath the North Patagonian Massif with respect to both; the surrounding backarc and the arc crust.

Márquez, 1999; Jordan et al., 2001). Afterward, magmatic activity along the NPB reappeared in the upper Miocene with the emplacement of gabbros and leucogranites and the development of present day stratovolcanoes in the magmatic arc.

Studies based on ocean floor magnetic anomalies (Cande and Leslie, 1986; Pardo Casas and Molanr, 1987; Somoza, 1998; Somoza and Ghidella, 2005) show that for most of the Paleogene period, the convergence between ocean and continental plates at the latitude of northern Patagonia occurred at a very small angle ($<15^\circ$), and the Farallon–Aluk active ridge reached the South American plate developing a triple junction. However, at about ~ 23 Ma the Farallon plate split into the Cocos and Nazca plates to the South and Juan da Fuca plate to the North as a result of global rearrangement of plate boundaries (Lonsdale, 2005), and the convergence angle increased to the extent that it became almost perpendicular to the subduction front. This Paleogene interval of Farallon–Aluk–SAM triple junction and of small angle convergence is coincident with the magmatic activity gap in the NPB and the eastward shifting of the calc-alkaline magmatism to the position formerly occupied by the back arc.

2.2. The role of the North Patagonian Massif in the back arc

A further striking distinctive feature of the Northern Patagonian Andean segment is the presence of the North Patagonian Massif (NPM), located at 400 km east of the trench (Fig. 2A). Gravity data (Tassara and Yáñez, 2003) suggest a ~ 40 km thick crust beneath the NPM and a normal (~ 35 km) thickness in the surrounding back arc and fore arc (Fig. 2B). The NPM has remained undeformed by Cenozoic tectonics, other than vertical faulting, drag folds of the sedimentary cover (Coria et al., 1975), and uplift as shown by the marine Maastrichtian–Danian undeformed to slightly tilted sediments that cover the 1200 m height of the NPM. This suggests that the NPM has behaved as a thicker crustal block with respect to the back arc that is easily deformed by the Neogene tectonics.

In order to understand the tectonic role of the NPM it is necessary to underline some of its geomorphologic features that constrain its uplift history. The surface of the geological ensemble in the NPM formed by Paleozoic basement rocks and mid-Jurassic volcanic rocks shows a large planation surface (Aragón et al., 2010; González Diaz and Malagnino, 1984) that is interpreted as resulting from widespread upper Jurassic and Cretaceous erosion. Most of the broad planation surface of the NPM as well as the surrounding back arc was covered by shallow marine sediments of Danian–Maastrichtian age. These undeformed marine sediments are useful to determine the uplift history of northern Patagonia as a first constraint, since the 100,000 km² of the NPM block between the Gastre, Limay, Gualicho and Los Chacays lineaments (Fig. 2A), show the undeformed Danian–Maastrichtian marine sediments lying now at 1200 m above sea level, with respect to the deformed marine sediments lying at 500–700 m above sea level in the surrounding back arc surface. The second constraint to the uplift history of the NPM is the Somon Cura Plateau basalts (Fig. 2A) (SCPB; Kay et al., 1993). These late Oligocene basalt lavas spill as cascades from the top of the plateaus of the NPM to the surrounding back arc. Therefore the NPM uplift occurred sometime between the upper Paleocene and upper Oligocene. A third constraint is that in the back arc that surrounds the NPM contains the upper Paleocene–Eocene (EPEB) and Oligocene (WOB) synextensional volcanism and between them the development of Ñirihua basin (ÑB Fig. 2A); NPM uplift thus can be considered synextensional. With these constraints, it is argued here that even though the uplift of Northern Patagonia back arc started from mid Paleocene time, an Eocene or early-Oligocene uplift drove the NPM planation surface to an elevation of at least 500 m above the surrounding back arc to build a high-lying plateau, now at 1200–1400 m above sea level (Aragón et al., 2010). This uplift of the NPM is coeval with the extensional regime of the surrounding back arc and rules out a fold and thrust origin.

The work of Tassara and Yáñez (2003) based on gravity data, suggests that, compared to the surrounding back arc, the NPM crust is at least 7 km thicker and has a much greater elastic thickness (T_e) than the surrounding back arc crust, reaching 70 km (T_e) beneath the NPM root zone (Fig. 2B). The differences in rheology thickness imply large increases in lithosphere strength that may reach values of 10 times for a cratonic lithosphere compared with the adjacent back arc (Hyndman et al., 2005). Even though the NPM is not as cold or thick as a craton, these relative NPM/back arc thickness and rheology differences can account for the non-deformable mechanical behavior of the NPM with respect to the back arc. A second geological feature that has suffered little or no deformation in Eocene–Oligocene times other than rotation, extension and uplift, is the coastal block (Fig. 2; North Patagonian Batholith and Chilean Central Valley) that shows a normal crustal thickness (33 km) but very thick elastic thickness T_e (~ 70 km) (Tassara and Yáñez, 2003) with respect to the back arc.

2.3. The coastal blocks Tertiary rotation and drift history from paleomagnetic data

The present-day Nazca–South America plate boundary between 33 and 47°S shows a gently ocean-ward convex curvature nearly centered on the position of the NPM and the Loncoche area (Fig. 1). The deformations of the Benioff plane around the NPM is also recorded in the

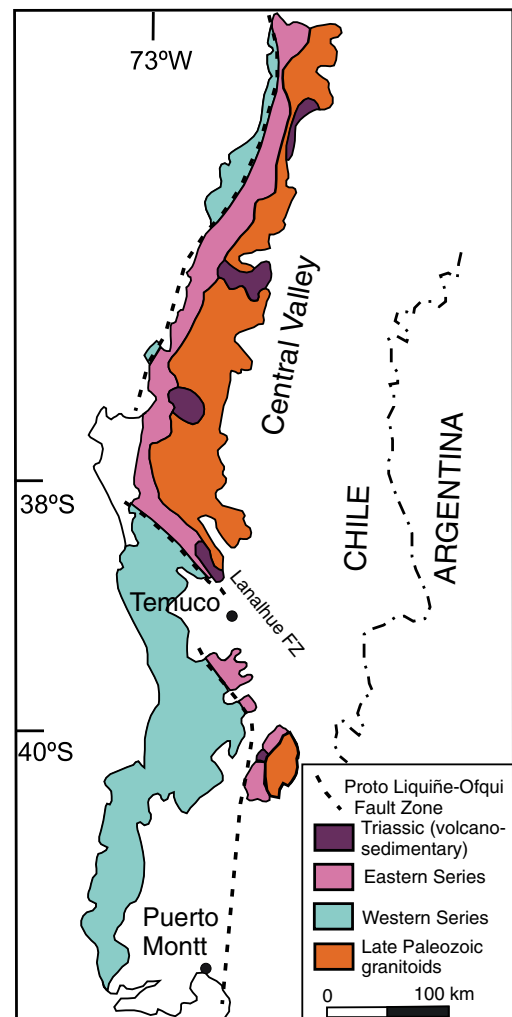


Fig. 3. Schematic Geological map of pre-Jurassic units in South Central Chile (Modified from Hervé et al., 2007). Showing docking of the Peninsular block (thickened Western Series) at Temuco area, and along the Proto Liquiñe–Ofqui Fault Zone. The Llanahue Fault Zone is a reactivation of the curved segment of the Proto Liquiñe–Ofqui Fault Zone.

Table 1
Selected major-element and trace element analyses of lavas and ignimbrites from Río Chubut Medio Volcanic field.

	Pre-caldera tholeiites		Caldera collapse ignimbrites				Intracaldera calc-alkalic volcanism													
	PN-2-06	PN-5-06	QL 9801	QL 9802	QL 9803	QL 9807	LP 17	LP 19	LP 20	LP21	LP 22	LP 23	EPP-T	EPP-1	EPP-B	EPP-6	Di-EPP	R-1	IGESC8682	IR-1-04
SiO ₂	55.09	58.72	77.61	79.83	87.68	85.06	56.64	61.54	58.20	55.37	60.18	60.35	70.11	77.51	76.73	76.89	79.23	82.72	73.72	78.94
TiO ₂	1.60	1.44	0.09	0.08	0.07	0.18	1.25	1.00	1.13	1.32	1.00	0.99	0.47	0.11	0.12	0.12	0.10	0.08	0.21	0.21
Al ₂ O ₃	15.63	17.06	11.34	10.11	6.32	7.23	16.55	15.75	16.20	16.81	16.00	16.03	14.27	12.11	12.61	12.53	11.49	9.56	16.81	12.45
Fe ₂ O ₃	9.75	8.77	3.36	2.14	1.55	2.51	7.89	6.32	7.35	8.24	6.57	6.41	4.92	1.76	1.94	1.90	1.14	0.76	1.93	1.69
MnO	0.24	0.06	0.02	0.02	0.01	0.01	0.11	0.11	0.08	0.14	0.09	0.11	0.10	0.03	0.04	0.04	0.01	0.01	0.03	0.01
MgO	3.78	1.71	0.41	0.23	0.20	0.71	4.43	3.25	4.29	4.58	3.60	3.58	0.32	0.08	0.04	0.05	0.06	0.01	0.02	0.16
CaO	7.91	5.30	2.88	1.16	1.42	1.54	6.33	4.41	5.97	6.65	5.39	5.14	2.09	0.53	0.49	0.47	0.37	0.13	0.86	0.52
Na ₂ O	4.03	4.38	3.18	5.49	1.73	1.22	4.29	4.81	4.33	4.64	4.24	4.41	3.81	3.67	3.48	3.32	3.60	2.80	2.41	3.36
K ₂ O	1.60	2.17	1.08	0.91	0.96	1.49	2.23	2.56	2.16	1.93	2.69	2.75	3.82	4.18	4.52	4.66	3.97	3.88	3.89	2.59
P ₂ O ₅	0.38	0.38	0.02	0.02	0.08	0.06	0.30	0.25	0.28	0.31	0.24	0.22	0.11	0.02	0.02	0.02	0.02	0.03	0.13	0.08
Total	100	100	100	100	100	100	100	100	100	100	100	100	100	100	100	100	100	100	100	100
Ba	262	286	21	14	86	421	310	383	310	349	394	368	1011	671	779	740	834	580	699	462
Sr	427	411	104	35	139	58	162	224	305	422	280	321	174	18	60	16	60	14	60	293
Y	27	25	19.2	27.7	15.9	28.1	23	28	25	25	29	30	57	74	70	66	54	37	49	38
Sc	19	16					16	13	15	17	14	14	11	2	<1	<1	<1	<1	<1	<10
Zr	220	256	1070	896	475	531	207	282	234	206	289	294	453	341	363	346	301	275	334	192
V	214	189	8	8	4	21	131	92	118	145	102	100	<5	<5	<5	<5	<5	<5	13	19
Cr	82	77	<20	<20	35	<20	65	43	62	72	294	55	<20	<20	<20	<20	<20	<20	61	2
Co	47	28	6	2	3	12	27	22	27	29	25	21	17	12	18	26	18	25		10
Ni	46	43	<15	<15	169	<15	67	45	69	70	287	31	24	<15	<15	23	<15	21	4	6
Cu	30	44	11	12	<10	<10	32	17	29	33	28	23	<10	<10	<10	<10	<10	<10	3	10
Zn	83	71	334	313	131	153	59	56	70	71	65	53	91	135	112	122	66	40		131
Ga	20	22	27	22	22	17	23	20	19	21	20	19	24	23	25	24	24	19		24
Rb			179	18	125	112	262	60	45	62	61	42	275	181	85	189	85	111	157	
Nb	12	15	52.9	47.5	28.8	25.7	18	21	19	18	24	22	33	40	39	39	35	28	25	32
Cs			12.3	14.3	20.6	7.6	0.5	1.2	0.8	0.6	1.2	1.4	17	9.4	6.1	6.6	2.9	2.5		
Hf			32.3	25.1	11.7	13.3	5	6.7	5.7	5	6.9	7.1	12	10	11	10	8.8	8.4		
Ta			9.1	7.6	3.4	4.2	1.5	1.9	1.6	1.5	2.2	1.9	3.1	3.38	4	4.4	3.7	4.3		<10
Pb			5	<5	5	5	<0.5	<0.5	5	<0.5	5	<0.5	9	22	10	11	9	6		<2
Bi			<0.06	<0.06	<0.06	0.07	0.19	0.1	0.11	0.14	0.15	0.11	0.64	<0.05	0.49	0.55	0.42	0.12		
Th			11.4	17.8	6.53	7.44	4.43	6.5	4.88	4.04	6.47	6.55	10.4	12.8	13.5	13.3	11.8	10.2	25	
U			2.5	1.45	3.5	1.03	1.04	1.55	1.2	0.99	1.62	1.62	2.43	3.32	3.26	3.53	3.31	1.58		
La	24	26	3.3	17.3	14.5	14	21.6	21.6	22.5	22.1	26.2	26.4	55.4		50.3	56.1	54.6	44.2	55	47
Ce			12.2	37.2	34.3	33.8	45	53	45	43	52	52	114		103	112	115	90	118	
Pr			1.08	5.06	4.1	3.99	4.98	5.66	5.05	4.93	5.82	5.76	12.4		11.6	12.2	12.4	10		
Nd			4.52	22.7	15.5	15.5	22.3	24.7	22.2	23.1	24.7	24.2	52.9		51.2	54.4	52.6	44.1		
Sm			1.69	6.98	4.27	4.47	4.94	5.56	4.9	5	5.32	5.07	12.3		11	12.1	12.3	9.57		
Eu			0.143	0.458	0.255	0.72	1.526	1.35	1.368	1.498	1.305	1.309	1.824		2.715	2.035	1.861	1.38		
Gd			2.5	6.02	3.53	4.53	4.38	4.91	4.35	4.77	5.04	5.13	11.3		10.1	10.8	10.9	8.36		
Tb			0.55	1	0.62	0.88	0.78	0.88	0.81	0.83	0.89	0.93	2.14		1.86	2.04	2.03	1.53		
Dy			3.51	4.99	3.36	5.46	4.24	5.03	4.39	4.37	4.94	4.91	12		9.97	11.6	10.8	7.83		
Ho			0.75	0.92	0.61	1.12	0.83	1.03	0.84	0.86	0.99	0.94	2.33		1.94	2.25	1.95	1.43		
Er			2.03	2.44	1.63	3.25	2.39	2.85	2.47	2.44	3.04	3.04	6.82		5.73	6.4	5.43	4.06		
Tm			0.304	0.344	0.239	0.471	0.328	0.437	0.382	0.356	0.428	0.449	1.008		0.878	1.005	0.828	0.609		
Yb			1.78	1.89	1.56	2.93	2.24	2.8	2.48	2.24	2.75	2.69	6.54		5.27	5.91	5.1	3.49		
Lu			0.243	0.24	0.204	0.442	0.298	0.401	0.306	0.288	0.39	0.42	0.878		0.735	0.819	0.543	0.392		
Sr87/Sr86i			0.7036	0.70591	0.70331	0.70367	0.70714			0.70393		0.70952	0.70426				0.70389	0.70711		
La/Yb			1.85	9.15	9.29	4.78	9.64	7.71	9.07	9.87	9.53	9.81	8.47		9.54	9.49	10.71	12.66		
Zr/Y			55.73	32.35	29.87	18.9	9	10.07	9.36	8.24	9.97	9.8	7.95	4.61	5.19	5.24	5.57	7.43	6.82	5.05
Ba/La	10.92	11	6.36	0.81	5.93	30.07	14.35	17.73	13.78	15.79	15.04	13.94	18.25		15.49	13.19	15.27	13.12	12.71	9.83
Nb/La	0.5	0.58	16.03	2.75	1.99	1.84	0.83	0.97	0.84	0.81	0.92	0.83	0.6		0.78	0.7	0.64	0.63	0.45	0.68
Y + Nb			72.1	75.2	44.7	53.8	41	49	44	43	53	52	90	114	109	105	89	65	74	70
La/Th			0.29	9.97	2.22	1.88	4.88	3.32	4.61	5.47	4.05	4.03	5.33		3.73	4.22	4.63	4.33	2.2	
La/Ta			0.36	2.28	4.26	3.33	14.4	11.37	14.06	14.73	11.91	13.89	17.87		12.57	12.75	14.76	10.29		
Ba/Rb			0.12	0.78	0.69	3.76	1.18	6.38	6.89	5.63	6.46	8.76	3.68	3.71	9.16	3.92	9.81	5.23	4.45	

<15 = below detection limit.

Table 1 (continued)

	Post-caldera tholeiites																	Post-caldera alkalic basalts						
	99-4	99-9	CE-1	ES-00-3	ES-PILL	99-12	CE-2/9801	ES-00-6	99-2	ES-00-14	CE-98-05B	CE-4-B	CE-4-N	CE-98-02	ES-00-9	ES-99-13C	ES-99-13B	ES-99-13A	VC-21-04	VC-25-04	VC-6	ZEB-1-04	ZEB-4-04	ZEB-5-04
SiO ₂	51.95	55.13	57.24	53.30	53.61	61.59	59.05	60.31	60.35	61.22	66.58	66.85	67.77	67.24	66.59	67.86	69.7	66.58	50.30	48.13	47.54	53.00	54.19	55.75
TiO ₂	1.45	1.52	1.55	1.39	1.58	1.39	1.56	1.30	1.32	1.04	0.68	0.99	0.69	0.78	0.67	0.70	0.70	0.75	1.26	0.95	2.74	1.52	1.93	1.53
Al ₂ O ₃	16.97	18.44	17.69	16.64	16.49	17.01	16.91	15.79	16.40	16.83	16.45	16.96	16.56	17.79	16.92	16.21	16.29	16.08	16.74	16.90	16.54	17.17	16.44	17.34
Fe ₂ O ₃	9.56	4.85	4.97	9.49	9.77	0.45	5.57	7.26	6.82	6.25	3.86	3.27	1.76	1.48	3.07	3.20	1.28	2.16	11.29	12.33	13.54	9.09	10.01	7.35
MnO	0.17	0.14	0.13	0.15	0.24	0.13	0.18	0.18	0.08	0.12	0.14	0.07	0.09	0.04	0.05	0.10	0.05	0.05	0.16	0.16	0.18	0.13	0.12	0.18
MgO	6.30	4.89	4.47	5.12	4.26	3.14	3.00	2.93	2.59	2.84	0.70	0.64	0.57	0.17	0.31	0.35	0.19	0.19	7.12	9.02	5.48	5.01	3.65	3.11
CaO	8.81	9.92	7.58	9.11	8.37	10.81	6.65	4.98	4.82	5.85	1.77	1.95	1.51	1.58	1.15	1.41	1.50	1.46	9.12	9.62	7.86	8.55	7.21	8.06
Na ₂ O	3.55	3.86	4.35	3.89	4.36	3.39	4.97	5.07	4.96	4.74	5.71	5.38	6.10	6.68	5.69	6.16	5.90	8.71	3.17	2.65	3.92	3.97	4.50	4.77
K ₂ O	0.79	0.88	1.61	0.91	1.34	1.61	1.71	2.16	2.25	1.11	3.97	3.55	4.80	4.07	5.56	4.02	4.35	4.01	0.57	0.16	1.58	1.19	1.48	1.58
P ₂ O ₅	0.45	0.38	0.41	N.D.	N.D.	0.48	0.40	N.D.	0.43	N.D.	0.15	0.34	0.14	0.18	N.D.	N.D.	N.D.	N.D.	0.26	0.08	0.61	0.38	0.48	0.34
Total	100	100	100	100	100	100	100	100	100	100	100	100	100	100	100	100	100	100	100	100	100	100	100	100
Ba	184.5	245	283	235	235	241	344	353	351.1	255	522	528	521	578	585	545	548	556	168	32	411	606	311	257
Sr	410	534	473	609	437	392	332	436	381.1	521	160	219	159	206	182	175	179	205	537	463	521	532	513	401
Y	20	22	25	23	33	18	38	30	28	23	48	40	51	48	41	40	38	36	22.7	13.7	31.3	21.6	25	25.5
Sc	26	10	13	20	23	9	16	11	16	10	8	7	16	8	6	5	<5	7	30	26	25	27	23	27
Zr	142	150	186	179	246	126	303	295	256	214	694	442	581	729	614	240	144	240	112.5	33.5	194.2	166.4	191	230.7
V	184	176	147	186	191	85	121	111	112	106	9	23	10	17	9	9	11	15	191	156	244	179	223	183
Cr	161	71	51	90	92	56	22	47	13	44	<20	2	<1	<20	30	28	30	28	146	243	27	8	11	2
Co	45	36	36	45	45	34	35	26	26	37	22	10	61	13	32	3	2	3	47	56	41	18	35	34
Ni	103	34	37	32	22	27	15	10	7	26	<15	10	14	<15	6	<1	<1	<1	84	158	48	14	15	8
Cu	39	39	40	51	35	49	16	31	14	23	<10	22	<2	<10	6	3	3	6	38	44	37	13	72	24
Zn	80	80	73	107	112	66	89	105	71	116	106	225	87	71	164	98	54	142			109			
Ga	18.6	15	12	17	17	2	5	18	19.2	18	23	24	21	25	23	24	24	25	16.6	13.5	20.8	18.2	20.8	20.4
Rb	22	7	28			19	39		46.2		83		79	64					10.8	4.6	29	18.8	15.9	12.3
Nb	11.3	14	20	10	21	10	29	23	23.2	3	43.5	56	53	46.1	19	51	51	53	7.4	0.5	26.8	16.6	20.1	20.5
Cs											1.4			0.2										
Hf	3								5		14.5			14.8					2	1	3	3	3	4
Ta	1.6			<10	<10			<10	2.1	<10	4.9	<10		4.5	<10	<10	<10	<10	0.9	0.3	2.2	1.6	2.2	1.7
Pb	12	18	23	4	<2	21	18	<2	15	8	6	2	29	9	16	14	3	27	<2	<2	<2	17	<2	<2
Bi				<5	<5			<5		<5	<0.6	<5		<0.6	<5	<5	<5	<5						
Th	3.8	3	2			5	11		13.4		8.41		11	8.79					5.7	2.5	3.5	2.6	3.3	1.7
U	0.4	<1	1			<1	1		1.4		2.41		3	2.96					0.1	0.1	0.6	0.8	1	0.9
La	26.2								21.3		44.4			48					29.6	0.5	18.2	16.3	24.8	23.4
Ce											92.9			98.2										
Pr	5.7								7.5		10.2			10.8					3.3	1	7.2	5.4	6.8	5.8
Nd	22.3								27.4		38.5			41					13.9	5	27.9	21.4	27.7	22.2
Sm	5								5.8		7.99			8.24					3.4	2.1	6.7	5.3	6	4.9
Eu	1.5								1.7		2.12			2.34					1.3	0.8	2.2	1.5	1.8	1.8
Gd	4.9								6.2		7.34			7.59					4.2	2.8	6.8	5.2	6	5.8
Tb	0.7								0.9		1.38			1.37					9.7	0.4	1	0.7	0.8	0.7
Dy	3.7								5.2		8.07			7.99					4.3	2.6	5.8	4.2	4.9	4.7
Ho	0.8								1		1.63			1.6					0.8	0.5	1.2	0.8	0.9	0.9
Er	2.2								2.8		5.07			4.86					2.3	1.5	3.2	2.2	2.6	2.7
Tm	0.3								0.4		0.81			0.81					0.3	0.2	0.5	0.3	0.4	0.4
Yb	1.6								2.6		5.33			5.16					2.1	1.2	2.8	2	2.3	2.5
Lu	0.2								0.4		0.83			0.8					0.3	0.2	0.4	0.3	0.3	0.4
Sr87/Sr86i	0.7																							
La/Yb	16.37								8.19		8.33			9.3					14.1	0.42	6.5	8.15	10.78	9.36
Zr/Y	7.1	6.82	7.44	7.75	7.46	7	7.97	9.96	9.14	9.13	14.46	11.17	11.39	15.19	14.95	5.97	3.77	6.73	4.96	2.45	6.2	7.7	7.64	9.05
Ba/La	7.04								16.48		11.76			12.04					5.68	64	22.58	37.18	12.54	10.98
Nb/La	0.43								1.09		0.98			0.96					0.25	1	1.47	1.02	0.81	0.88
Y+Nb	31.3	36	45	33.43	54.06	28	67	52.13	51.2	26.13	91.5	95.58	104	94.1	59.67	91.23	89.39	88.68	30.1	14.2	58.1	38.2	45.1	46
La/Th	6.89								1.59		5.28			5.46					5.19	0.2	5.2	6.27	7.52	13.76
La/Ta	16.37								10.14		9.06			10.67					32.89	1.67	8.27	10.19	11.27	13.76
Ba/Rb	8.39	35	10.11			12.68	8.82		7.6		6.29		6.59	9.03					15.56	6.96	14.17	32.23	19.56	20.89

continental crust by the clockwise and counter clockwise fore arc block rotations with respect to a center corresponding to the Loncoche area in Chile (Fig. 1B). The fore arc to the north of Loncoche area has Cretaceous ash-flow tuffs and upper Tertiary tuffs with paleomagnetic data that show a Neogene 14° clockwise rotation (Beck et al., 1986; Vietor et al., 2004; Vietor and Echter, 2006) since the beginning of subduction of the Nazca plate in the middle Miocene. Instead, the fore arc to the south of the Loncoche area (Peninsular Block, which comprises the Puerto Montt Peninsula and the Chiloe Island) and North Patagonian Batholith granites and mafic dikes to the west of the Liquiñe–Ofqui fault have paleomagnetic data from Oligocene–early Miocene volcanic rocks that show a Neogene 14° counter-clockwise rotation with little internal deformation (Beck et al., 2000; Rojas et al., 1994).

Furthermore, paleomagnetic data show that the southern peninsular fore arc (Fig. 2, south of the Loncoche area) has moved northward by about 400 km in early Tertiary time (Beck et al., 2000; García et al., 1988). The thickened Eastern Series south of the Loncoche area and Temuco (Fig. 3) suggest that this is the docking area of the northward drifting peninsular block. The fault system that separates the eastern from the western series runs along strike with the plate margin and can be related to a Paleogene Proto Liquiñe–Ofqui transcurrent fault system. At the latitude of Temuco, a strong S inflection of the Proto Liquiñe–Ofqui fault develops a Transverse Range that separates the Central valley to the north with respect to the Puerto Montt embayment to the south. This oblique fault system is now reactivated by the Lanahue fault system.

Further considerations can be made regarding this Paleogene active plate margin and the Paleogene extensional setting of northern Patagonia. Contrary to the Neogene coastal block rotations north and south of the Loncoche area, paleomagnetic data for upper Mesozoic plutonic rocks to the east of the Liquiñe–Ofqui fault suggest (for the Paleogene) mainly counter clockwise rotation to the north of Loncoche and mainly clockwise rotation to the south of Loncoche (Fig. 1B) (Beck et al., 2000; García et al., 1988). Thus a rotation reversal of the coastal blocks occurred by about middle Miocene time, and can be correlated with the Farallon plate break up that gave rise to the Nazca plate, and the tectonic reversal of the extensional Paleogene faults during the Neogene compressive event shown by Jordan et al. (2001), Charrier et al. (2002), Giacosa and Márquez (1999).

3. Geochemical features of synextensional Paleocene–Eocene volcanism

Voluminous calc-alkaline volcanic activity developed during Paleogene more than 400 km east of the plate margin (Rapela et al., 1983; Rapela and Kay, 1988) under an extensional tectonic setting (Giacosa and Heredia 2004; Mancini and Serna, 1989; Rapela et al., 1983; Rapela and Kay, 1988; Silvestro and Zubiri, 2008). This Paleogene volcanism is related to the development of the Ñirihuau basin (Cazau et al., 1989; Spalletti, 1983). In the Paleogene calc-alkaline volcanism, two main belts of volcanic activity are recognized (Fig. 2A); an eastern late Paleocene–Eocene belt (EPEB) and the Western Oligocene belt (WOB) (Rapela et al., 1987).

The eastern upper Paleocene–Eocene belt (EPEB) is composed of bimodal calc-alkaline volcanic rocks (basalt–rhyolite) with large amounts of ignimbrites and a subordinate amount of andesites and basalts toward the top of the sequence (Rapela et al., 1987). Most radiometric ages range from 60 to 42 Ma (Rapela et al., 1983). In the EPEB volcanic rocks, the rhyolites and dacites predominate as large ignimbrite plateaus and subordinate domes, lava flows and subvolcanic rocks (Aragón and Mazzoni 1997; Rapela et al., 1987). Small amounts of tholeiitic basalts that evolve to trachyte (Aragón et al., 2004b) and alkali basalts (Aragón et al., 2005) are present towards the top of the sequence. The WOB volcanic rocks also start as dacite–rhyolite flows and ignimbrites and become more andesitic to basaltic to the top of the sequence.

Representative rocks from the EPEB have been sampled for geochemical characteristics in order obtain additional information

regarding tectonic events during the Paleogene in this sector of the North Patagonian region. The results will be contrasted with geological and geophysical data. This study is based in a detailed sampling of the volcanic rocks at the Río Chubut medio area (Fig. 2A, and Table 1), since it shows a complete and well age-constrained sequence of the EPEB (Aragón and Mazzoni, 1997), with the complete range from calc-alkaline rhyolites and andesites, tholeiitic basalts and trachytes and alkali basalts.

3.1. Sampling and analytical techniques

3.1.1. Sampled units

A total of 45 samples from the EPEB at the Río Chubut medio area were collected for geochemical characterization. These include basalts, andesites, trachytes and rhyolites. A total of 200 samples were collected for petrographic study.

Fig. 4 shows a vertical section of volcanic activity in the EPEB that has been summarized as Pre-caldera, Caldera and Post-caldera stages.

The Pre-caldera volcanic rocks are tholeiitic basalts with zoned plagioclase, augite and chloritized olivine in a devitrified groundmass, and have a K/Ar radiometric age of 57.8 Ma (Mazzoni et al., 1991).

At the Caldera stage, the most abundant volcanic products by far are rhyolitic ignimbrites related to a 25 km diameter collapse caldera with an erupted volume of more than 300³ km (Aragón and Mazzoni, 1997). These ignimbrites form a large plateau, with a maximum thickness of about 100 m and remnant outcrops covering an area of about 400 km². Two main units can be distinguished. The lower unit is characterized as being composed of high silica rhyolitic (sanidine free), and poorly welded undeformed pumice ignimbrites. The upper unit consists of high silica rhyolites and highly welded ignimbrites with fiamme. Both units have volcanic, plutonic and metamorphic lithoclasts and a small amount of small crystal clasts (2 mm diameter).

Andesites rocks composed of zoned plagioclase, augite and groundmass, form necks, feeders, sills and etmoliths of 1 to 50 m thickness. Rhyolites are almost aphyric, with small amounts of microporphyritic anorthoclase. They form glassy perlithic domes of

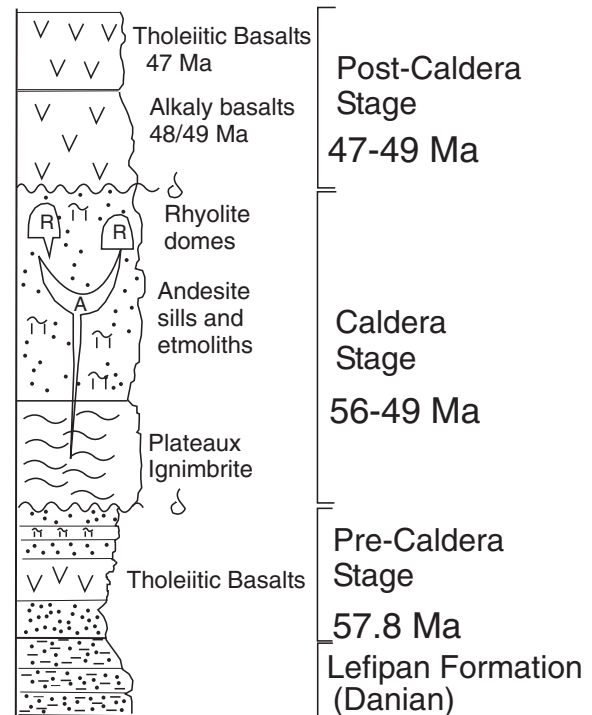


Fig. 4. Schematic lithostratigraphic column of the EPEB at the study area, related to the caldera and ignimbrite flare-up stage. The continental EPEB lies upon Danian estuarine silts of Lefipan Formation.

200 to 400 m diameter and 80 m thickness and devitrified foliated rhyolite domes of 200 to 500 m diameter and 100 m thickness (Aragón et al., 2001, 2004a). The K/Ar radiometric ages of these caldera collapse ignimbrites and intracaldera calc-alkaline lavas range from 56 to 49 Ma (Mazzoni et al., 1991; Wilf et al., 2005).

The Post-caldera sequence is formed by tholeiitic and alkalic lava flows. The tholeiitic basalts spread over an area of 100 km² and have an average thickness of 200 m. They evolve to trachytic ignimbrites. Basalts are microporphyritic rocks with a dominant assemblage of olivine altered to bowlingite, zoned plagioclase, and diopside rich augite-rimmed hypersthene (Aragón et al., 2004b) and have a K/Ar radiometric age of 47 Ma (Mazzoni et al., 1991).

The alkali basalts form the last Paleogene volcanic episode in the region. These spread inside and outside the caldera over an area of 350 km² and have an average of 50 m thickness. They are characterized by microporphyritic olivine, augite and zoned plagioclase

(Aragón et al., 2005), and have ⁴⁰Ar/³⁹Ar radiometric ages of 48 to 49 Ma (Gosses et al., 2006).

3.1.2. Analytical techniques

Analyses were carried out on rocks with no alteration and clear phenocrysts. For ignimbrite rocks hand picking of ground mass and pumice was performed to eliminate foreign lithoclasts. Major element analyses were performed by ICP, and trace elements by ICP-MS. The samples with full REE determination were performed by Neutron Activation.

3.2. Results of the geochemical study

3.2.1. Major elements

Geochemical data (Table 1; Fig. 5) of the EPEB show that calc-alkaline and tholeiitic rocks major element compositions do not differ

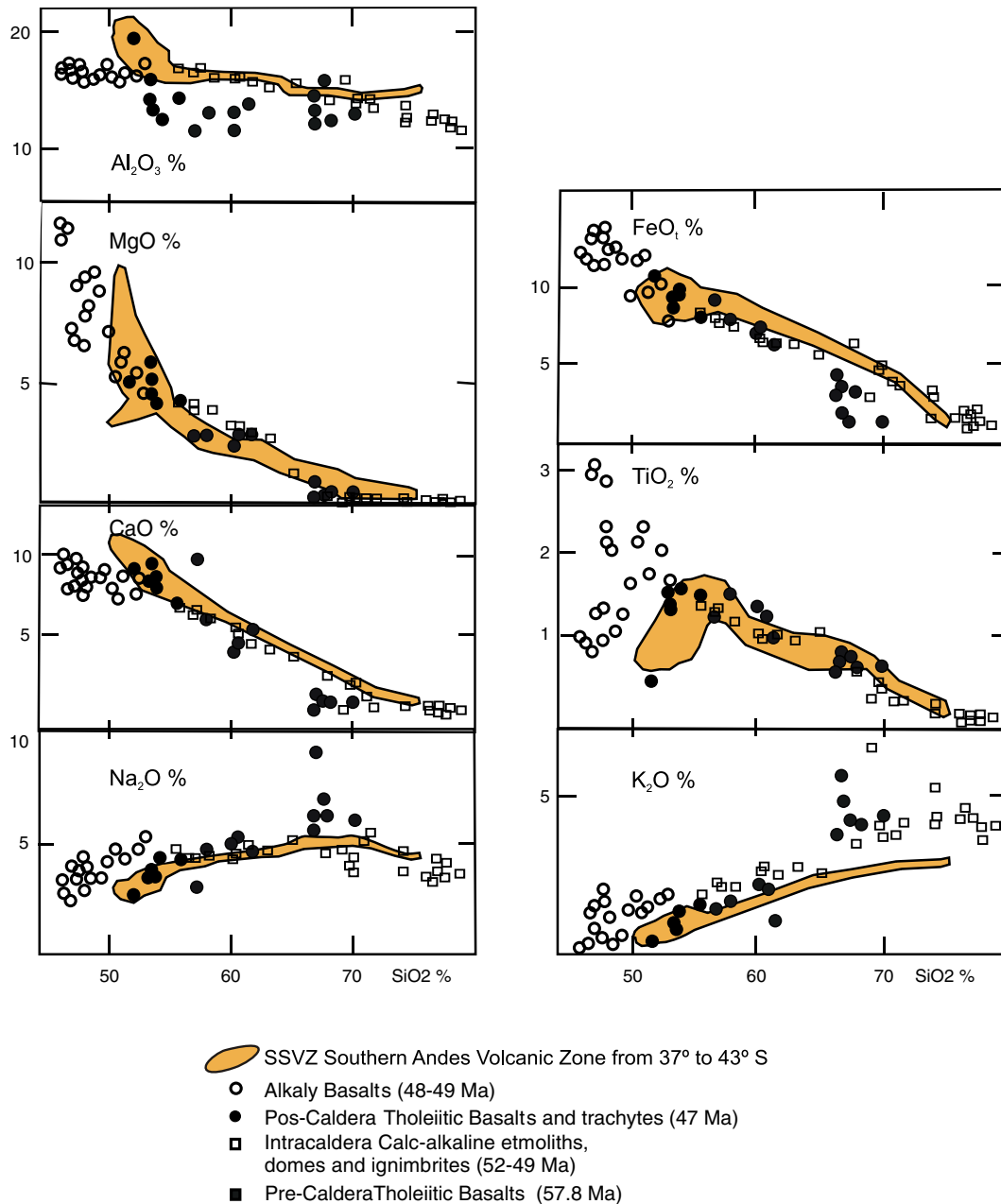


Fig. 5. Major elements versus SiO₂ diagrams for samples from the EPEB. The orange field show the Neogene volcanic arc at the same latitude (SVZ rocks), plotted as reference in all diagrams. Data of SVZ is from Gerlach et al. (1988), Lopez Escobar et al. (1991), López-Escobar et al. (1992), Mella et al. (2005), and Tormey et al. (1991).

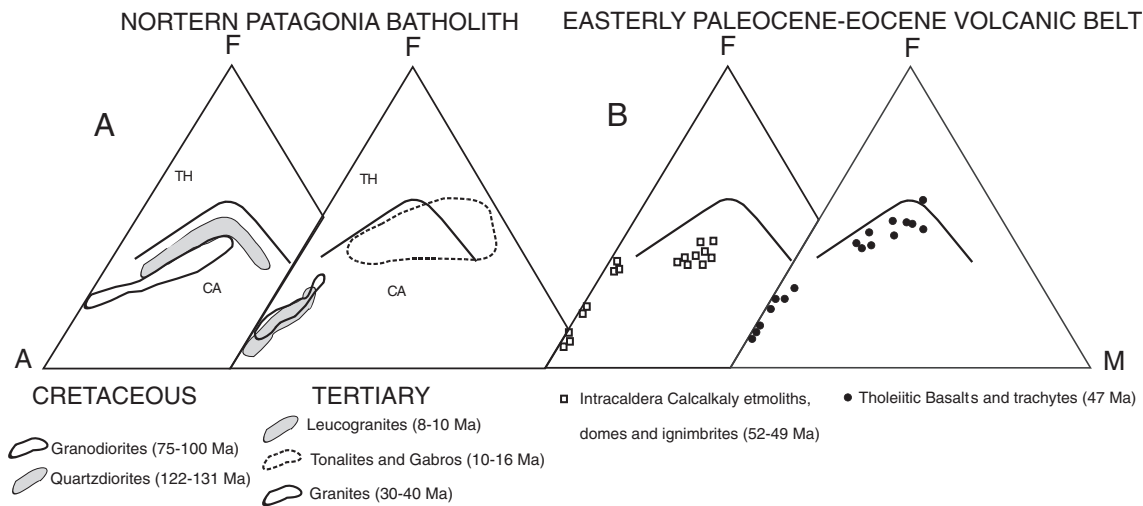


Fig. 6. AFM diagrams with the calc-alkaline (CA) and tholeiitic (TH) fields, to show temporal and compositional variations of: A) Northern Patagonian Batholith plutonic rocks with respect to; B) the EPEB volcanic rocks at the same latitude of the active margin. North Patagonian Batholith data is from Rapela and Kay (1988).

much from the present day Southern Andes Volcanic Zone (SVZ) southern segment (37° – 43° S) volcanism and the Tertiary northern (38° – 43° S) segment of the North Patagonian Batholith (NPB) (Fig. 6). The pre- and post-caldera basalts show a tholeiitic trend in the FeO^*/MgO versus SiO_2 diagram (Fig. 7; Miyashiro, 1974) but this is not so evident when considering the alkalis, as in the AFM diagram (Fig. 6). The post-caldera tholeiitic basalts and andesites are also associated with trachytes, and alkali basalts (Ne normative hawaiites, Fig. 7). The

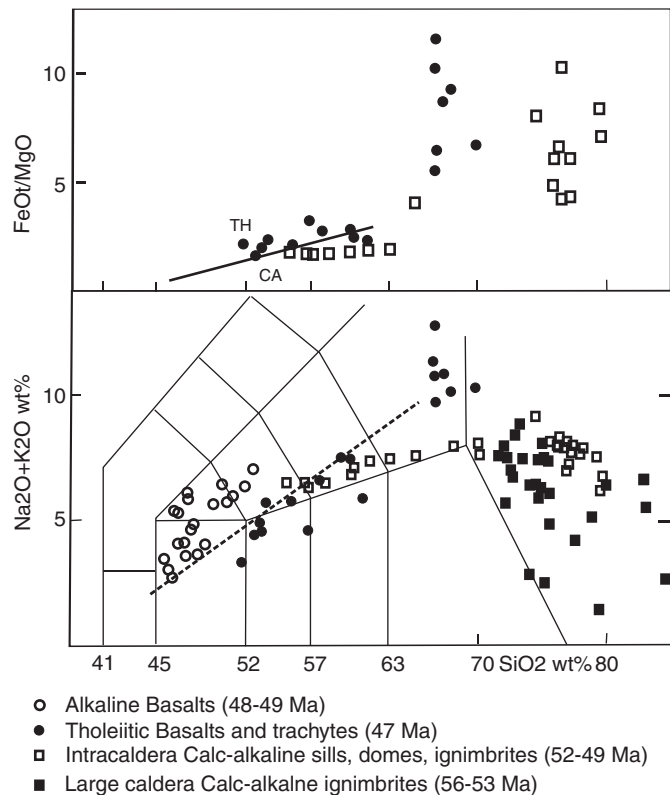


Fig. 7. Total alkalis and FeO^*/MgO versus SiO_2 for the rocks of the EPEB. The fields for alkalic and subalkalic and for tholeiite and calc-alkaline are from MacDonald (1968) and Miyashiro (1974).

Caldera stage shows trachy-basalts, andesites, dacites (in the trachyte transition) and rhyolites of calc-alkaline nature (Fig. 7).

The most outstanding differences between EPEB and SVZ are that EPEB calc-alkaline and tholeiitic rocks show normal to high K_2O contents, that are much higher than those of present SVZ arc compositions (Fig. 5), and that EPEB tholeiitic rocks have a much lower Al_2O_3 content with respect to calc-alkaline volcanics (Fig. 5).

3.2.2. Trace elements

Large ion lithophile (LIL) Ba, Rb of the EPEB have similar concentrations to the NPB and the SVZ (Fig. 8), for a given Silica content (Fig. 9), but are relatively enriched in high field strength (HFS) incompatible elements such as Nb, Ta, Y (Figs. 8 and 9). The EPEB calc-alkaline and tholeiitic rocks have incompatible element ratios $\text{Ba}/\text{Nb} < 30$; $\text{Ba}/\text{La} < 15$; and $\text{Nb}/\text{La} > 0.5$ values which are not of orogenic andesites (Gill, 1981) and are much lower than those of SVZ basic rocks (Table 1; Fig. 10).

Similar (but not so sharply) low incompatible trends in volcanic centers from behind the Andean SVZ volcanic front, compared to those along the front, have been associated with a lower input of fluids derived from the subducted Nazca plate below the front (Hickey-Vargas et al., 1986, 1989; López Escobar et al., 1977, 1976, 1992, 1993, 1995; Stern, 1991). But, this is not so for the EPEB since the Ba content for both EPEB and SVZ is the same for any given silica

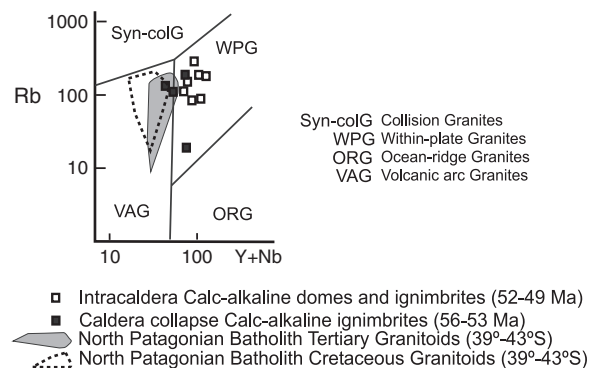


Fig. 8. Rb versus $(\text{Y} + \text{Nb})$ discrimination plots for the main Cretaceous and Tertiary plutonic igneous units of the North Patagonian Batholith compared with respect to the EPEB volcanic rocks. Different granites types fields after Pearce et al. (1984). Granitoids data is from Cingolani et al. (1991).

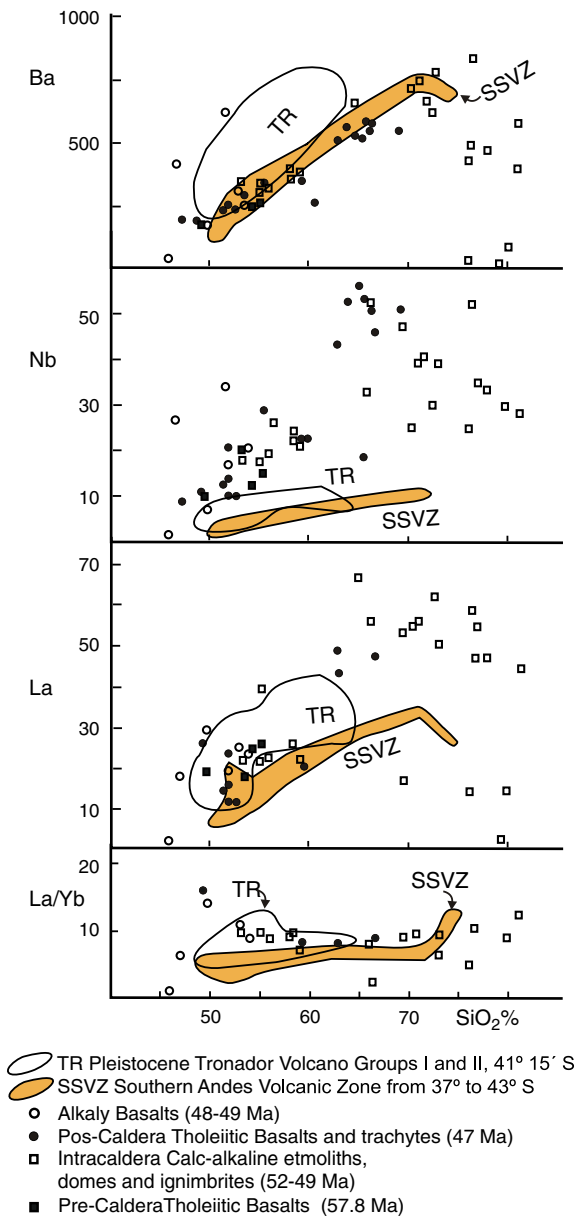


Fig. 9. Ba, Nb, La and La/Yb versus SiO₂, for rocks of the EPEB, compared with respect to the southern segment of the SVZ rocks (orange field) and Tronador volcanic arc rocks (TR) at the same latitude at the active margin of the South American plate. The SVZ and Tronador data is from Gerlach et al. (1988), Lopez Escobar et al. (1993), Mella et al. (2005), and Tormey et al. (1991).

content (Fig. 9). The low Ba/Nb ratios of the EPEB is due to the higher Nb contents (Fig. 9)

The relation between HFS incompatible and LIL trace elements of the NPB (upper Cretaceous–Tertiary) and the EPEB (Fig. 8) shows a slight HFS enrichment in the Tertiary plutons of the batholith that suggest an overall transition to a more HFS rich Paleogene igneous rocks.

The Th–Ta–Hf/3 diagram (Fig. 11) shows that Ta of EPEB volcanics are enriched with respect to a Th and Hf (high-Ta/Hf ratio), the WOB volcanic rocks also show a Th decrease with respect to a medium-Ta/Hf ratio. Instead the SVZ remains with a low Ta/Hf ratio, as expected in volcanic arcs.

REE patterns of the EPEB subalkalic rocks (Fig. 12) are relatively flat with light REE enrichment of with respect to heavy REE (except

for the lower unit of the caldera collapse ignimbrite). The EPEB La/Yb (8–10) ratios are relatively constant as SiO₂ increases (Fig. 9), and are slightly higher than the southern segment of the SVZ (Cf. López Escobar et al., 1977; Tormey et al., 1991) but much the same as the Pleistocene Tronador lavas (Cf. Mella et al., 2005). In this respect López Escobar et al. (1977), Tormey et al. (1991) considered the La/Yb variations along-strike the SVZ to be a consequence of crustal thickness, melting degree and depth of magma source variations, and the southern segment of the SVZ represents the thinnest crust, largest degree of melting and shallowest magma source (garnet free mantle) regions of the SVZ. The EPEB has higher La concentrations than the SVZ, but similar La concentrations to the La rich (Group II, of Mella et al., 2005) Pleistocene Tronador volcanic rocks (Fig. 9). The lower Yb contents and higher La/Yb ratios of the EPEB suggest the presence of garnet in the source and a deeper mantle source for these magmas with respect to the southern part of the SVZ, and similar to the group II of the Pliocene Tronador volcanic rocks as proposed by Mella et al. (2005) for these rocks.

Subalkalic basaltic and andesites samples do not have a Eu anomaly, although dacites through most rhyolites show a slight Eu anomaly, and the ignimbritic rhyolites of the caldera collapse show a strong Eu anomaly. The alkali basalts show a wide range of REE patterns and of La/Yb (0.42 to 14) ratios with OIB affinity.

3.2.3. Sr isotopes

Sr isotopic ratios were determined on EPEB volcanic rocks (Table 2). Isotopic analyses were conducted at the Centro de Pesquisas Geocronológicas (Universidade de São Paulo, Brasil), and the Sr concentration at the Centro de Investigaciones Geológicas (Universidad Nacional de La Plata, Argentina) as described by Cingolani et al. (1993).

Initial Sr isotopic ratios EPEB range between 0.70331 and 0.70952. The lower value is presented by a voluminous caldera collapse ignimbritic rhyolite and the higher by the andesite etmolith. The Sr isotopic ratios of rocks from the EPEB are independent of their SiO₂ and Sr contents (Table 2, Fig. 13), and show a flat pattern close to the 0.7035 ratio. The higher values are few and related to the andesitic sills and etmoliths (within caldera magmatism).

4. Seismicity and tomography

The distribution of earthquake hypocenters (Fig. 1A) is one of the most reliable methods by which to constrain the geometry of the subducting slab at depths between 50 and 200 km. The seismic pattern of the South America active margin from the Triple Junction at the Taitao Peninsula in Southern Chile to Peru (Fig. 1A) shows along-strike differences related to the subduction of the Nazca plate that are also visible in the 3D regionalized upper mantle (RUM) seismic model of South America (Fig. 1B; Gudmundsson and Sambridge, 1998). These marked regional differences are the well known flat-slab segments of central Chile and central Peru (heavy bracket in Fig. 1B) and the adjacent segments of normal ($\approx 30^\circ$) subduction (Barazangi and Isacks, 1979).

The age of the Nazca plate increases steadily from the south (4 Ma at 45°S) to the north (48 Ma at 20°S; Fig. 1A). As oceanic plate age increases so should lithospheric thickness and plate subduction angle on the one hand, while subducted plate buoyancy decreases on the other. Nevertheless, the Andes have alternating along strike normal and flat-slab segments apparently uncorrelated to this first-order relationship (Fig. 1B). Variation of the subduction angle is possibly induced by variability of crustal buoyancy, independent of the age of the subducted slab and influenced by the local morphology and tectonics of the subducting plate (Gutscher et al., 2000). The present seismogenic zone beneath northern Chile appears as a large continuous belt for more than 600 km, extending to a depth >300 km (zone of increased hypocenter density in Fig. 1). In contrast, northern Patagonia and southern Chile

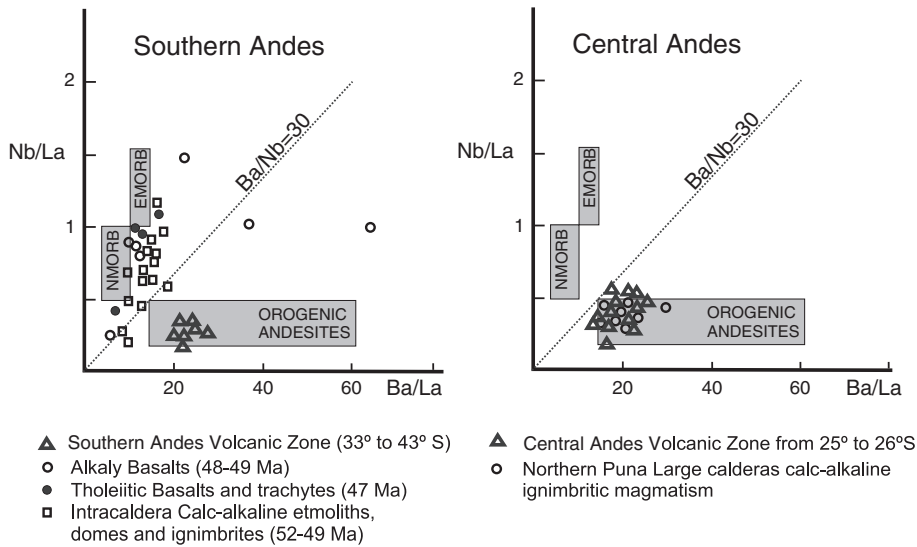


Fig. 10. Nb/La versus Ba/La diagrams. A) to demonstrate the relatively high Nb and low Ba contents of the northern Patagonia EPEB ignimbrite flare-up with respect to the present active arc volcanism (SVZ) at the same latitude. B) The Central Andes Puna ignimbrite flare-up and its active arc volcanism (CVZ) relationship, for comparison with EPEB ignimbrite flare-up. Notice that contrary to northern Patagonia, both; Puna's back arc ignimbrite flare-up and arc volcanism at the CVZ have the same Nb and Ba ratios typical of orogenic andesites. The SVZ data is from Lopez Escobar et al. (1993), and Tormey et al. (1991). The CVZ and Puna ignimbrites are from de Silva (1991) and Walker et al. (1991).

show a much narrower seismogenic zone (Fig. 1), with the Benioff plane only reaching a depth <200 km. Such a tectonic configuration probably reflects a quasi-steady condition since 23 Ma break-up of the Farallon plate (Yáñez et al., 2002).

Tomographic sections are another reliable means of imaging subducted lithosphere using perturbations of p-wave velocities in the mantle (Bijwaard and Spakman, 2000; Bijwaard et al., 1998) fast velocities = dense, cold lithosphere; slow velocities = hot, light material below 100 km depth typically asthenosphere).

Previous tomographic models interpretations of the neighboring areas of northern Patagonia, such as Gutscher et al. (2000), have used

tomographic models to study the flat-slab segments at the central Andes, and Heintz et al. (2005) have evaluated tomographic resolution and worked with new improved shear wave tomographic models of southern South America to suggest a shallow-slab segment at the austral Andes

In northern Patagonia, the tomographic model of a vertical cross section (Fig. 14A) passing through the NPM, shows a moderately dipping fast velocity anomaly that coincides with seismic hypocenters and continues to a depth of 350–400 km, and that can be interpreted as the subducting Nazca plate lithosphere. From 400 km the fast velocity anomaly is no longer present. A fast velocity anomaly is re-

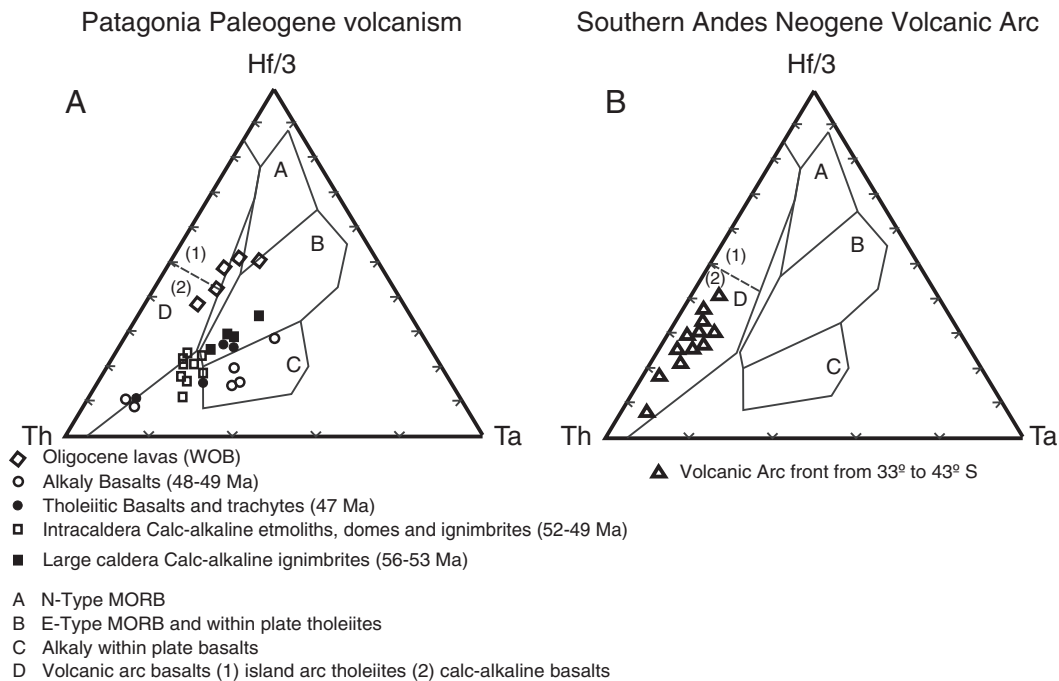


Fig. 11. The Th–Hf–Ta discrimination diagram (after Wood, 1980) to show the different behavior of the calc-alkaline volcanic rocks of A) the EPEB and WOB, with respect to B) SVZ arc volcanoes at the same latitude. Notice that the EPEB large caldera ignimbrites (ignimbrite flare-up) plot in the E-MORB-within plate tholeiitic field. The SVZ data is from Lopez Escobar et al. (1993), and Tormey et al. (1991).

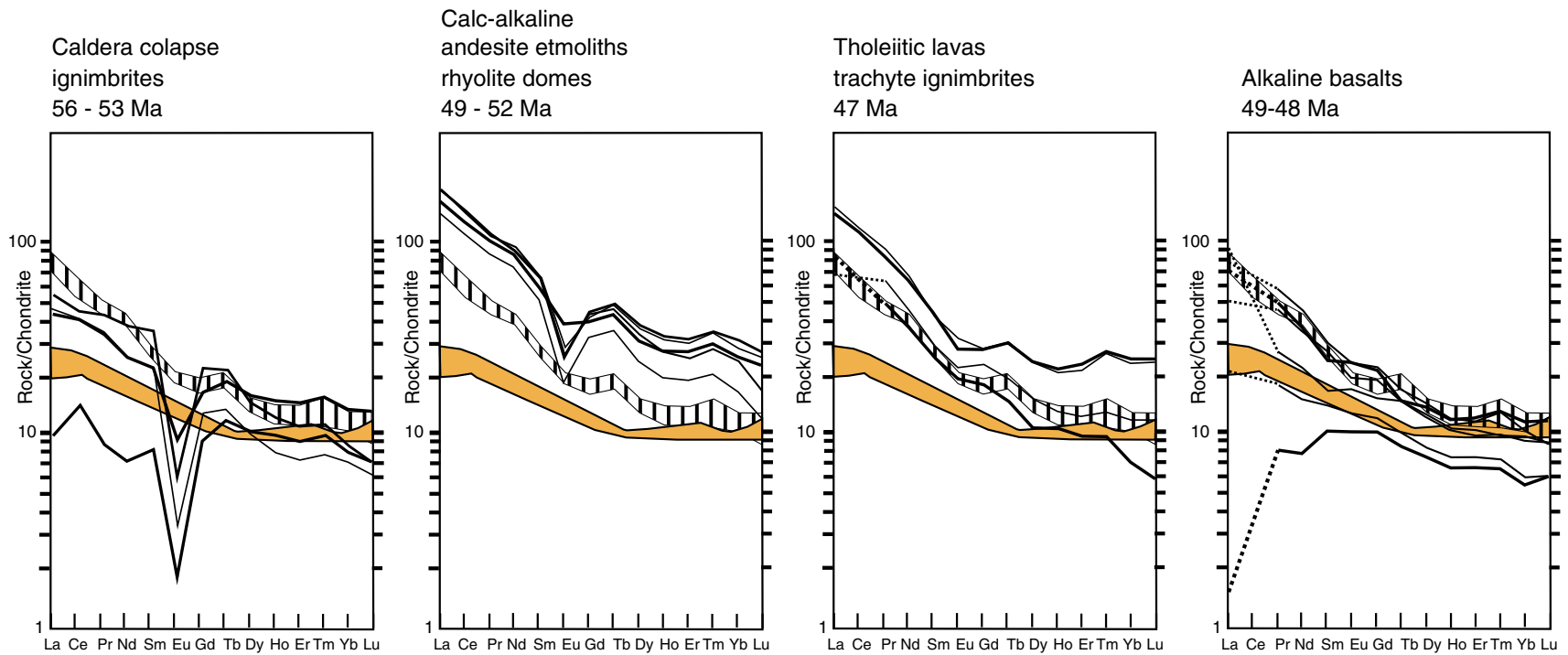


Fig. 12. Chondrite-normalized REE patterns for the EPEB rocks, A) Caldera collapse ignimbrites. B) Intra-caldera calc-alkaline andesites and rhyolites. C) Post-caldera tholeiitic basalts. D) Post-caldera alkaline basalts. Gray field is for Intra-caldera calc-alkaline andesites; Orange field is for SVZ basalts, plotted as reference in all REE diagrams. Field for the SVZ volcanic front is represented by data from Gerlach et al. (1988) and Hickey-Vargas et al. (1986).

Table 2
Selected Sr isotopic analyses of lavas and ignimbrites from Río Chubut Medio Volcanic field.

	Field N°	Rb (ppm)	Sr (ppm)	Rb ⁸⁷ /Sr ⁸⁶	Error	Sr ⁸⁷ /Sr ⁸⁶	Error	Age (Ma)	Sr ⁸⁷ /Sr ⁸⁶ (i)	SiO ₂
Caldera collapse ignimbrite	QL 9801	179.3	103.7	50,054	0.1001	0.707507	0.000011	55	0.7036	77.61
	QL 9803	124.5	138.5	26,017	0.052	0.70534	0.00001	55	0.70331	87.68
	QL 9802	18	35	1,488,742	0.029775	0.707073	0.000021	55	0.70591	79.83
	QL 9807	111.9	58.1	55,758	0.1115	0.708031	0.000022	55	0.70367	85.06
Intracaldera calc-alkalic volcanism	LP 21	41.4	422	0.2839	0.0057	0.704141	0.000014	52	0.70393	55.37
	LP 23	62.2	321.3	0.5606	0.0112	0.709939	0.000014	52	0.70952	60.35
	LP 17	261.8	162.2	46,739	0.0935	0.710589	0.000019	52	0.70714	56.64
	8655	106	82	3,741,826	0.074836	0.706523	0.000019	50.9	0.70382	69.29
	DI EPP	85	60	4,100,835	0.082017	0.706829	0.00002	50.5	0.70389	79.23
	EPP T	274.6	174	45,986	0.092	0.707501	0.000015	50	0.70426	70.11
	IGES8682	157	60	7,578,155	0.151563	0.711784	0.000021	50	0.70711	73.72
Post caldera basalt flows	99-4	22	410	0.155276	0.005743	0.703524	0.000017	47.2	0.70342	51.95
	153	15	840	0.051675	0.005787	0.703603	0.000016	43.1	0.70357	47.71

established at a depth of 650–700 km that continues sub-horizontally along the ≈ 700 km depth for about 500 km. The lateral extent of the anomaly gap (Fig. 14F) and the 650–700 km isolated sub-horizontal fast velocity anomaly (Fig. 14G), show that these features occupy the whole with of the segment, and that are exclusive to this particular Andean segment when compared to the neighbor Andean segments (Fig. 14B, C, D, E, F and G). This shows an important lithospheric discontinuity for the Nazca plate in northern Patagonia followed by another possible lithospheric segment that we interpret as a remnant of ocean plate lithosphere.

The lack of continuity between the actively subducting slab (seismic hypocenters with the fast anomaly segment) with respect to the fast anomaly segment lying at ≈ 700 km in depth (for the whole with of the northern Patagonia segment), and the apparent different inclination of the deeper slice suggest that a slab detachment has occurred, rather than a simple slab break-off. Furthermore, using as a reference the distance between ocean floor ages at anomalies 5 (10.59 Ma), 13 (35.58 Ma) 18 (42.01 Ma) as seen within the neighboring transforms of the Nazca plate (Fig. 1), the age of the subducted lithosphere can be reasonably estimated (yellow circles in Fig. 14A) and from the position of the subducting front it can be estimated that subduction was re-established ~ 23 Ma ago. The magmatic activity of the associated arc had begun about 15 Ma ago (Munizaga et al., 1988) suggesting a ≈ 8 Ma long period to rebuild the subduction and suprasubduction steady state tectono-magmatic structure.

5. Discussion

5.1. The trace elements, isotopes, tectonic setting and tomography model assemble for the Paleogene

The EPEB has Ba, Rb and Sr concentrations similar to the SVZ that suggest a lithosphere enriched by subduction, but the large HFS Nb, Ta concentrations suggest a within-plate setting. This can be explained partly by the synextensional condition of this volcanism that suggests high degrees of decompression melting, with large volumes of silicic calc-alkalic magmatism (ignimbrite flare-up). This bimodal association of the calc-alkaline ignimbrite flare-up with a final stage of within-plate alkali basalts (some with mantle xenoliths, Alric et al., 2002) and tholeiitic basalts–trachytes also show the extensional origin of this magmatism. The voluminous synextensional EPEB in the former back arc is coeval with the Tertiary magmatic gap in the North Patagonian Batholith, suggesting a slab window or slab detachment setting and not a rollback or flat slab setting. Besides, the very small ocean–continental plate convergence angle and the collision of the Farallon/Aluk spreading ridge (unstable F–R–T–T quadruple junction Fig. 15) registered for the Paleogene (Cande and Leslie, 1986; Somoza, 1998; Somoza and Ghidella, 2005) at this latitude will evolve to a “transform” ocean–continental plate margin setting (F–R–T and F–F–T triple junctions Fig. 15), over ruling previous suggestions of small angle subduction (Kay and Rapela, 1987) for the Eocene. This is in agreement with the plate-detachment suggested by the tomographic model fast anomaly interpretation, which shows a possible detached lithosphere with a cut-off edge at 1000 km from the present trench. Thus, the late Cretaceous–early Paleogene detached lithospheric slice can be part of Farallon/Aluk plates.

A similar condition of a large synextensional calc-alkalic ignimbrite flare-up followed by tholeiitic and alkali basalts has been described in the Basin and Range Neogene magmatism (Gans et al., 1989; Hawkesworth et al., 1995; Hooper et al., 1995) and has been interpreted as decompression melting of a lithosphere enriched by a former subduction process (Hawkesworth et al., 1995).

As for most volcanoes along the SVZ, the Sr isotopic ratios of rocks from the EPEB are independent of their SiO₂ and Sr contents (Table 2, Fig. 13), but have unusually low Sr isotopic ratios in the high silica ignimbrites of the caldera collapse stage (ignimbrite flare-up), these ignimbrites are single eruptions with volumes of more than 300 km³ of rhyolites with little microporphyrific feldspar of 2 mm and absence of amphibole and biotite (Aragón and Mazzoni, 1997). In the SVZ the small Sr isotopic ratio variation is interpreted as a lack of significant amount of crustal assimilation in conjunction with fractional crystallization (Hickey-Vargas et al., 1989; Stern, 1991), this seems to be also the case for the EPEB but with the difference that the larger volumes of rhyolitic rocks with respect to basalts and fewer andesites

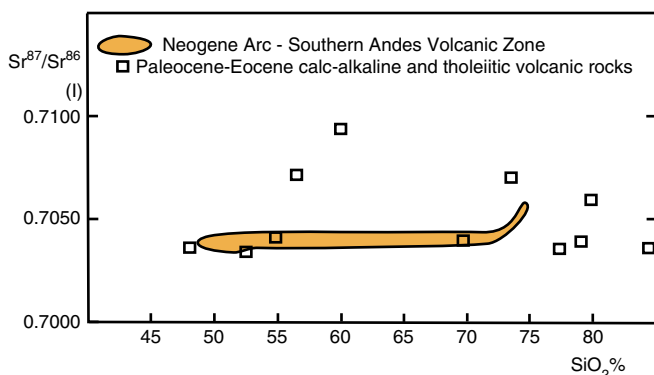


Fig. 13. Variations of initial Sr isotope ratios with SiO₂. The Easterly Paleocene–Eocene Belt (open squares) is compared with the volcanic arc SVZ (orange field is for SVZ rocks) at the same latitude. The SVZ data is from Gerlach et al. (1988), Lopez Escobar et al. (1993) and Tormey et al. (1991).

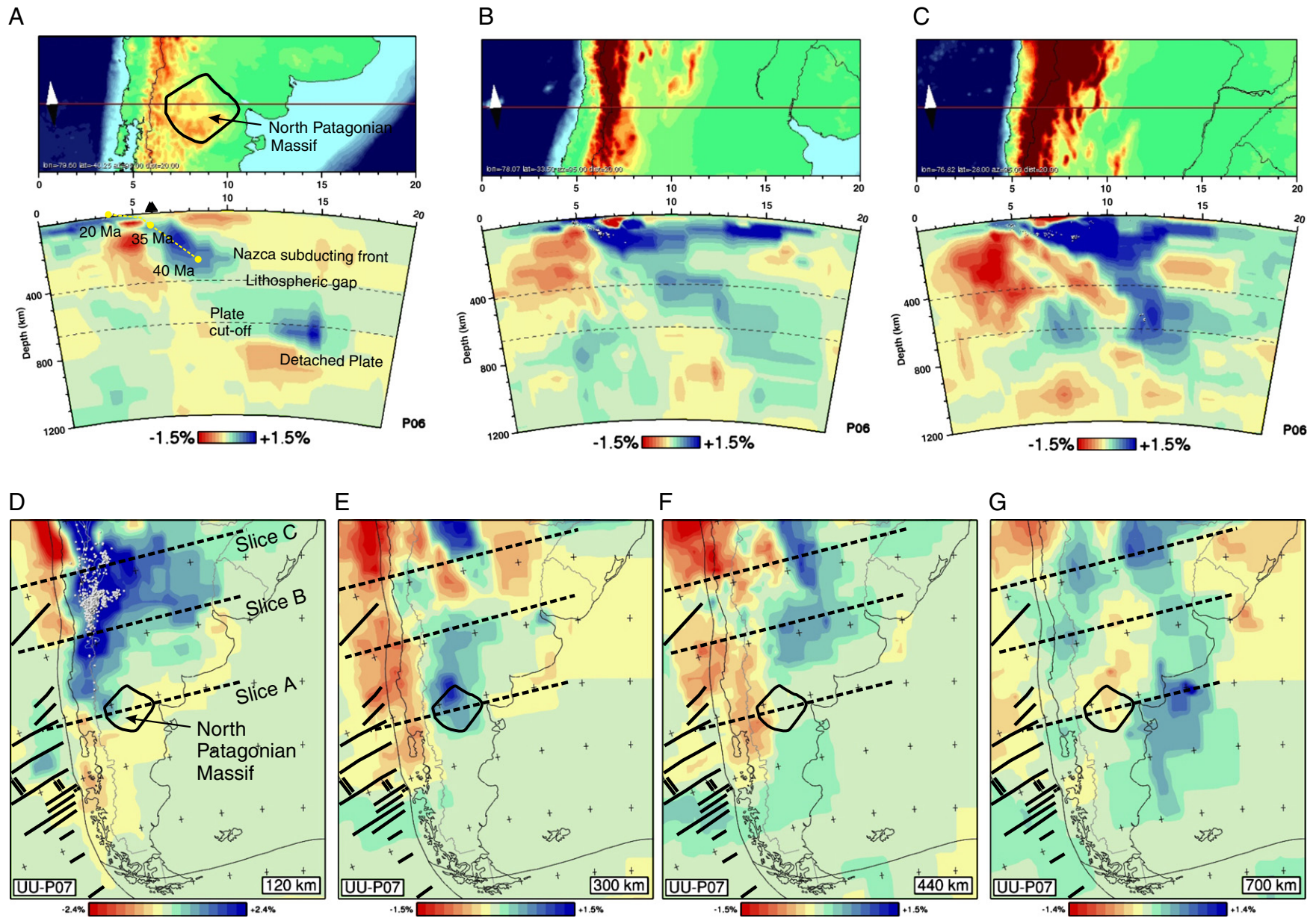


Fig. 14. Cross sections and maps from global tomographic model at the Latitude of Southern Andes (after Bijwaard et al., 1998, Bijwaard and Spakman, 2000). (A) Cross section at northern Patagonia showing normal subduction angle and a modeled fast anomaly discontinuity at the 350–600 km depth. White dots = Earthquakes hypocenters; dark blue = fast velocities = dense, cold lithosphere; red = light material; yellow circles, stippled line and numbers show estimated ages for the subducted Nazca Plate using the distances measured at the Nazca plate ocean floor known anomalies ages in Fig. 1. (B) and (C) cross sections at the neighbor segments to the north of Patagonia showing flat slab geometries and the modeled fast anomaly distributed along with the deep seated earthquakes hypocenters. (D), (E), (F) and (G) maps at 120, 300, 440 and 700 km respectively showing the segmentation and lateral extent of the modeled anomalies at each segment at the southern Andes, black stippled lines show locations of cross sections (slices) (A), (B) and (C). Notice at (F) for the northern Patagonia segment (stippled line slice (A)), the lateral extent of the fast anomaly gap, and at (G) the lateral extent of the isolated flat laying fast anomaly, showing that these two modeled features are characteristic to this Andean segment in all its lateral extent, and not a local feature.

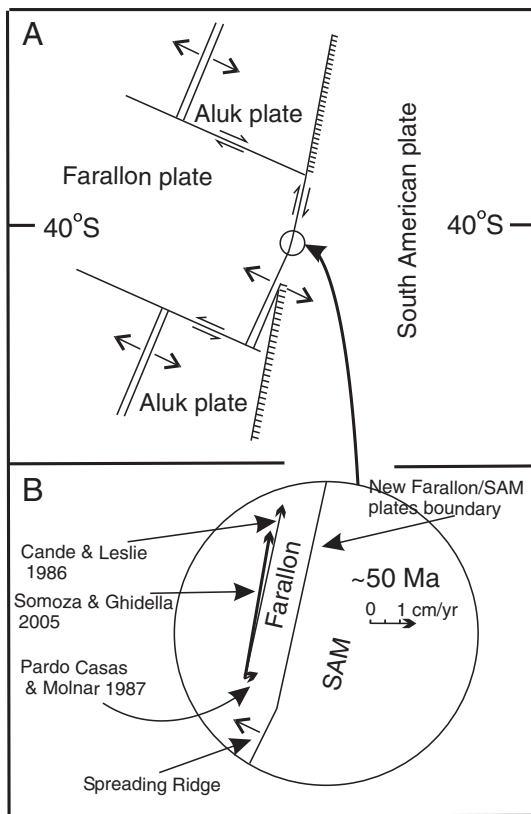


Fig. 15. Schematic reconstruction and evolution of the plate configuration in the Southern Andes during early the Eocene. Double lines indicate the Farallon–Aluk spreading ridge moving southwards (modified from Cande and Leslie, 1986, Somoza and Ghidella, 2005). (A) As the Farallon–Aluk spreading ridge reaches the trench, an unstable quadruple plate junction is formed which immediately evolves to two triple junctions; an R–F–T and a F–F–T type (R = spreading ridge, F = transform fault, T = trench). (B) Shows (at 40°S for the early Eocene) the relative motion of the Farallon plate to the South America plate (modified from Cande and Leslie, 1986, Somoza and Ghidella, 2005), and the convergence rate (Pardo Casas and Molnar, 1987). The very low relative motion angle between Farallon–SAM plates; the very low convergence rate at this latitude; and the high plate motion/plate convergence ratio 10/1; show that a new transform margin (Farallon–SAM plates) is the only possible solution to replace the old Aluk–SAM trench as the new Farallon–Aluk–SAM R–F–T triple junction migrate by the ongoing collision and southward drift of the spreading ridge with respect to the trench. The growth of this transform margin ends when the R–F–T triple junction evolves to an F–F–T triple junction.

suggest that batch melting may be more important than fractional crystallization.

The flat and low initial Sr isotopic ratios (0.7035) and the lack of phenocryst development of the EPEB ignimbrite flare-up suggest a young lithosphere and are consistent with a rapid movement of magmas through the crust, due to intense extension or related to a thinned crust in order to avoid crustal contamination and long-lived magma chamber emplacement.

Widespread extension and magmatism continues through Oligocene to lower Miocene with the development of the Ñirihuau basin (ÑB) between the NPM and the coastal block (Jordan et al., 2001; Spalletti, 1983). The Western Oligocene belt (WOB) is the western boundary of the Ñirihuau basin (ÑB Fig. 2A), and reflects bimodal calc-alkaline volcanism (basalt–rhyolite; Rapela et al., 1987) with OIB affinity (Kay and Rapela, 1987). These lavas have radiometric ages of 34 to 24 Ma (Cazau et al., 1989). To the west of the Andes, the Oligocene Coastal volcanic belt develops with OIB features and has been interpreted to show a slab window (Muñoz et al., 2000). To the east of the WOB, the broad Oligocene Somon–Cura basaltic plateau (SCBP) also has OIB and Arc affinities (Kay et al., 1993). In summary,

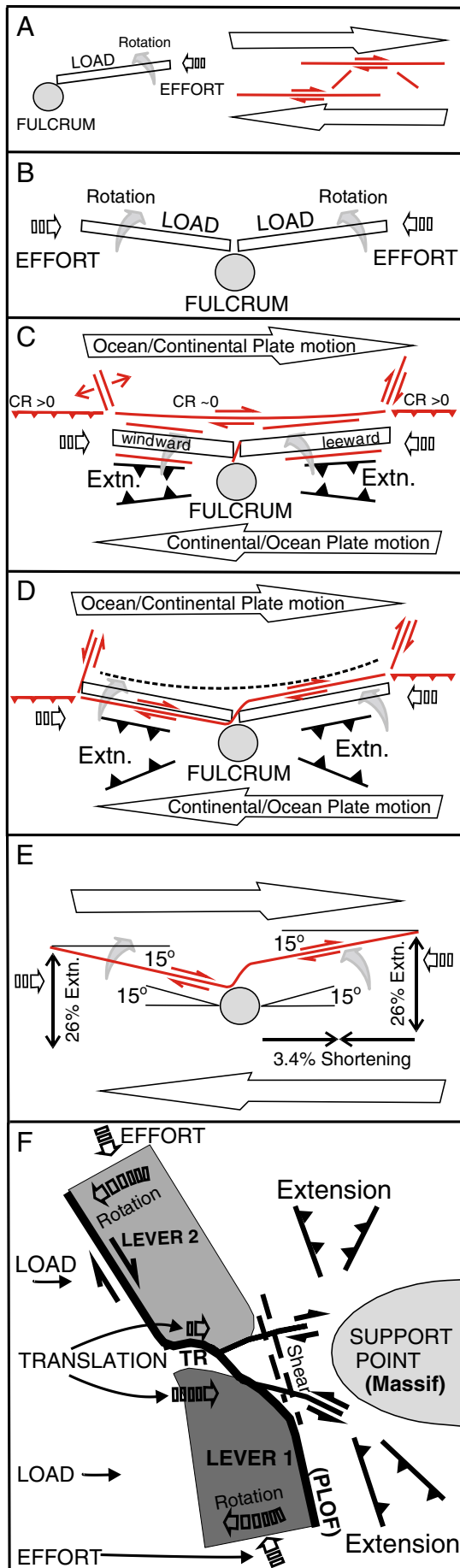
these broad Oligocene volcanic events throughout northern Patagonia show OIB and Arc affinity, that has been interpreted to be produced at local or regional scale by a hot spot (Kay et al., 1993; 2004) or slab window caused by slab roll-back (de Ignacio et al., 2001; Muñoz et al., 2000), or small angle subduction (Kay and Rapela, 1987). The Paleogene lithosphere detachment suggested by fast velocity anomalies of tomographic modeling and the within-plate geochemical evidence for the Eocene volcanism in this study suggest that the broad slab-window like Oligocene volcanism may be re-interpreted as the main stage of plate-detachment and extension that had started with the EPEB.

5.2. The synextensional-uplift in the former back arc

In addition to synextensional-calc-alkaline volcanism, northern Patagonia back arc experienced synextensional-uplift (Aragón et al., 2010). This is shown by the Eocene volcanic rocks with thin layers of sediments that are covered by the Eocene continental floras (Wilf et al., 2005). This Eocene uplift of the back arc is anomalous, in as much as homogeneous extension leads to isostatic subsidence rather than uplift. Subsidence in the back arc, fore arc and arc is finally attained by the upper Oligocene–lower Miocene with broad transgressions from the Atlantic and Pacific oceans respectively. Besides, in this back arc the NPM remained as a remnant block undeformed by extension, preserving the original thickened state, and contrary to the rest of the back arc history, it kept on suffering further uplift until it stood as a high plateau more than 500 m higher than the surrounding back arc in the late Oligocene. The continuous Paleogene uplift history of the NPM plateau is evidenced by the late Oligocene Somon Cura basalt lavas that overlie the Danian marine sediments (on top of the NPM) and spill (more than 400 m height difference) from the NPM plateau to the surrounding back arc. Thus the undeformed and thick NPM block is considered a “centralized” boundary for back arc crust deformation. In other words, the Paleogene extension and the Neogene tectonic inversion affected only the back arc crust surrounding the Massif. Given the closeness of the Massif to the plate margin (Figs. 2 and 13) it is suggested that it may have functioned as a support point for the forces produced by subduction or transcurrent plate margin relations in Cenozoic time.

5.3. The drift of the southern coastal block

The paleomagnetic data shows that the southern peninsular fore arc moved northward by about 400 km in early Tertiary time (Beck et al., 2000; García et al., 1988) bounded to the east by the Liquiñe–Ofqui fault zone. Beck et al. (2000) consider that the Liquiñe–Ofqui fault zone is a site of crustal decoupling, and the sliver of South America west of the fault is detached from the rest of the continent and has moved relatively northward without much internal deformation. To explain the northward transport of the peninsular block, Forsythe and Nelson (1985) proposed an ‘indenter’ model. Problems with this model are that such an indentation should have produced a symmetric equivalent of the LOF south of the triple junction and is too young to produce the 400 km displacement. To solve these problems Beck (1988) proposed an oblique subduction model. But, with the new evidence of the Paleogene ocean plate lithosphere gap beneath northern Patagonia (Fig. 14) and the coeval synextensional EPEB volcanism of within-plate affinity (Figs. 10 and 11), then the free fore arc block (Peninsular Block), its northward movement and the small plate-convergence angle for most of the Paleogene as the Farallon–Aluk spreading ridge collided with South America (Fig. 15), suggest a transcurrent plate margin setting during Paleogene along a Proto Liquiñe–Ofqui transcurrent fault (Fig. 16), rather than oblique subduction or Neogene indentation. It is also suggested that the docking of the Peninsular Block must be to the south of the Loncoche



area as indicated by the thickened Eastern Series and the deformation of the late Paleozoic and Triassic rocks at the Temuco area (Fig. 3) along oblique faults.

Now we can consider the Haschke et al. (2006) suggestion that the Paleogene extension and the synextensional widespread magmatism could be explained by retreat of the trench. Paleomagnetic data show clockwise and counter-clockwise coastal block rotation reversals with respect to the Loncoche area, and the detachment and northward migration of the fore arc Peninsular Block driven by very small plate-convergence angles, showing that the geometry of extension is ruled by the rotation of the coastal blocks with respect to a center promoted by a small angle convergence and not a uniform trench retreat.

5.4. The recovery of subduction

The end of the northern Patagonia ocean–continental plate transform margin is well documented as the Farallon plate breaks to give place to the Nazca plate coeval with a sharp change of ocean–continental plate convergence angle from very small to almost perpendicular at ~23 Ma ago (Cande and Leslie, 1986, Lonsdale, 2005). The change from transform to subduction regime can be also related to the tectonic inversion that occurs at mid–upper Miocene (Giacosa and Heredia, 2004; Giacosa and Márquez, 1999), the end of within-plate calc-alkaline magmatism, and the recovery in the upper-Miocene of arc magmatism in the North Patagonian Batholith followed by the development of the Southern Andes Volcanic zone.

5.5. Proposal of a new model

The tectonic model here proposed (Figs. 15, 16 and 17) considers the two coastal blocks to behave as facing lever arms (wheelbarrow type), having the NPM as a single central support point for both levers. The whole system reacts to subduction–transcurrence transition since the efforts change from perpendicular to parallel. Then, the Coastal Blocks (levers) with respect to the NPM (undeformable support point) are subjected to rotation reversal, causing extension during transcurrence (Figs. 16C and D; 17B and C), and compression (at the back arc) during normal subduction (Fig. 17D).

In this model the Proto Liquiñe–Ofqui fault represents the plate margin during the advance stage of transcurrence (when the F–R–T triple junction evolves to F–F–T, Fig. 16D). The trace of the main fault system has a strong inflection to the west of Loncoche (see * in Figs. 2A

Fig. 16. Schematic representation of the mechanical behavior of the two lever arms tectonic model (wheelbarrow type) at a transform margin. (A) To the left; a wheelbarrow type lever working with the effort almost parallel to the lever arm axis. To the right; a shear system (B) A double wheelbarrow type lever with a single fulcrum. (C) Young stage: showing major tectonic elements and efforts of the double lever transform margin and the bounding subduction margins that supply the effort for the levers. The clockwise rotation lever has a windward arm end and the counter-clockwise lever has a leeward arm end with respect to the ocean plate motion. CR = Convergence Rate. Extn = Extension. (D) Mature stage: As rotation continues and the R–T–F triple junction evolves to T–F–F type, the windward lever arm is decoupled and captured by the ocean plate. The transform margin jumps inland and the new transform fault has an S-shape. The decoupled windward lever arm is a microplate that docks towards the fulcrum. (E) Mechanical constraints of the double lever system. Measured rotation angles of coastal blocks in Chile (Beck et al., 1986, 2000) suggest that the Σ of counter and clockwise rotation angles can reach as much as 30° with respect to the compressive effort. This implies that the maximum extension this system may have reached is of 26% at the far end of the lever, decreasing towards the fulcrum, with a maximum of 3.4% of lateral shortening with respect to the levers length (because of tectonic reversal no data are yet available to verify this). (F) Details of the mature stage fault system at the levers/fulcrum junction (as in Fig. 17C Transform margin stage). The effort along-strike of the plate margin generates the transcurrent fault (PLOF = Proto Liquiñe–Ofqui Fault). The Coastal block breaks at the edge of the support point and develops a Transverse Range (TR) and a southern (1) and northern (2) lever, at each side of the transcurrent fault. The support point of the levers is the Massif. As counter-clockwise and clockwise rotation of the southern and northern coastal blocks proceeds, there is extension and crustal thinning at the former back arc.

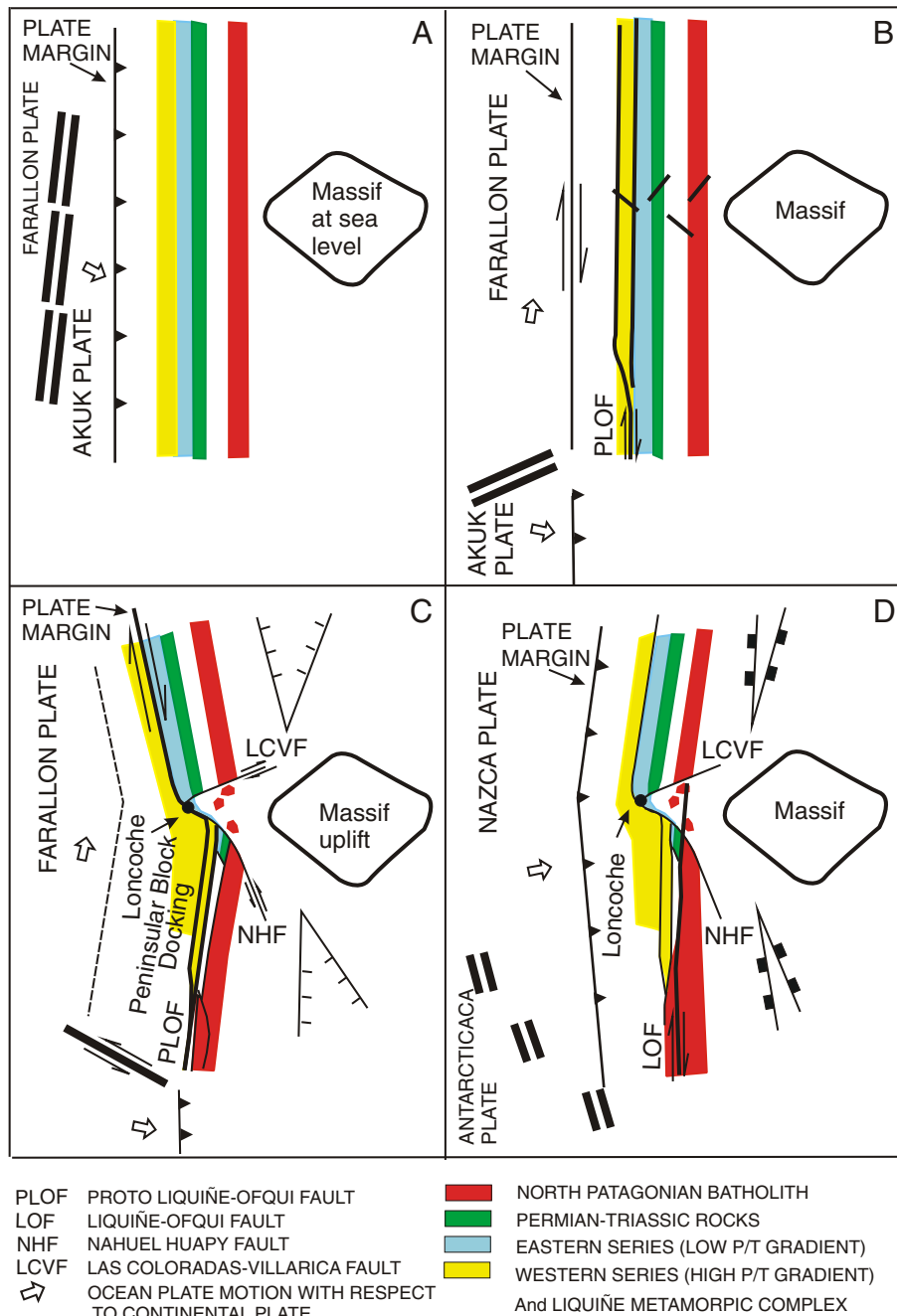


Fig. 17. Tertiary tectonic evolution model of northern Patagonia: A) In the Upper Cretaceous the Aluk plate is subducted. B) By late Paleocene–early Eocene, as the Farallon plate motion with respect the South American plate is close to parallel, the triple junction R–F–T caused by the collision and southward migration of the Farallon–Aluk spreading ridge develops a Paleogene transcurrent plate margin episode. Along-strike transcurrent faults (Proto Liquiñe–Ofqui fault system) start to develop inland. C) In the Oligocene, when the R–F–T triple junction evolves to an F–F–T triple junction, the transcurrent plate margin fault jumps inland and the Proto Liquiñe–Ofqui fault system has become the new plate margin. During this time the southern Peninsular block rotates clockwise and the Northern coastal block rotates counter-clockwise. Both block rotations induce a significant extension at the former back arc and fore arc, with the onset of synextensional calcalkaline–alkaline magmatism and crustal thinning. The massif is subject to strong uplift (with no deformation). In an early stage the Peninsular Block is dragged 400 km to the north by the transcurrent along the Proto Liquiñe–Ofqui fault. D) In Miocene time, the subduction tectonic setting is re-established with the break up of the Farallon plate to yield the Nazca plate with a high convergence rate with respect to the South American plate. The reversal of coastal block rotation is observed along with the tectonic inversion at fore arc, arc and back arc basins, the crustal thickening, and the re-establishment of the magmatic arc. The plate margin migrates westward to the trench joining the Peninsular Block to the South American Plate.

and 3) in correspondence with the support point of the two lever system. To the south the Proto Liquiñe–Ofqui fault allows the docking of the Peninsular Block and separates the metamorphic rocks of the Eastern Series (low P/T gradient) with respect to the Liquiñe Metamorphic Complex to the west (Western Series).

From Loncoche to the north the Proto Liquiñe–Ofqui fault runs in the Coast Range, separating the metamorphic rocks of the Eastern

Series (low P/T gradient) with respect to a narrow strip of the Western Series (high P/T gradient).

The transcurrent along the Proto Liquiñe–Ofqui fault accommodates the 400 km northward shifting of the Peninsular Block that is detached from the continental plate (Beck et al., 2000), under a very small plate convergence angle regime (Cande and Leslie, 1986). We interpret that the Peninsular Block moved together with – and thus

pertains to – the Farallon plate during transurrence. Vice versa it becomes integral with the South America plate during convergence when the plate margin migrates westward to the trench during the Neogene (Fig. 17C and D). The Peninsular region behaved therefore as a microplate. Presently this microplate behaves integrally with the South America plate.

Recovery of subduction at the plate margin causes the reversal of coastal block rotation, tectonic inversion in the fore arc, arc and back arc basins, crustal thickening, and the development of the magmatic arc.

6. Final considerations

The Paleogene magmatic history of Northern Patagonia shows a transition from arc to within-plate character. The northern segment of the North Patagonian Batholith diminishes intrusiveness rates to an upper Oligocene–lower Miocene magmatic gap. The upper Miocene recovery of magmatic activity in the batholith is accompanied by a change of composition to more gabbroic and leucogranitic end members. Coeval with the decrease of intrusiveness rate in the North Patagonian Batholith, the main magmatic activity migrated eastwardly to generate the EPEB volcanism with large volumes of silicic calc-alkalic magmatism (ignimbrite flare-up) with little or no crustal contamination, and associated with a final stage of alkali basalts (hawaiites) and tholeiitic basalts–trachytes. The synextensional and enriched in incompatible and HFS element-nature of the EPEB suggest a within-plate setting with high degrees of decompression melting of a lithosphere enriched by a subducted slab processes.

The extreme synextensional nature of the EPEB volcanism is also shown by the flat and low initial $\text{Sr}^{87}/\text{Sr}^{86}$ ratios from basalt to rhyolite. To the extent that microporphyrific rhyolite ignimbrite eruptions of more than 300 km^3 retain an initial $\text{Sr}^{87}/\text{Sr}^{86}$ ratio of 0.70331, showing that ascent was fast (did not allow crustal contamination), and that the back arc crust must have been thin or subject to crustal thinning by the extension.

The Oligocene is characterized by the maximum extension, with a widespread magmatism (from the Pacific to the Atlantic coasts) that includes the Coastal Oligocene belt, the western Oligocene belt and the Somon–Cura basaltic plateau (all with OIB affinity).

In addition, the tomographic modeling of northern Patagonia suggests a Paleogene subduction gap marked by an absence of fast anomaly continuity in the tomographic model (Fig. 14). This subduction gap is coeval with the collision of the Farallon–Aluk spreading ridge with South America at a very small ocean–continental plate convergence angle (Cande and Leslie 1986), and a continental crust break along the Liquiñe–Ofqui fault with 400 km northward drift of the coastal block (Beck et al., 2000; García et al., 1988), suggesting that the coastal block is attached to the Farallon plate and that a Transcurrent Plate Margin was developed in Paleocene time. Consequently we interpret that the plate margin jumps from the trench to the strike–slip fault system situated inside the continental plate (Proto Liquiñe–Ofqui Fault) when the Farallon–Aluk–SAM R–F–T triple junction evolves to a F–F–T triple junction (Figs. 16C and D; 17B and C). It appears therefore that the peninsular coastal block and outward accretion prism pertain to the oceanic plate during part of transurrence and to the continental plate during subduction (Fig. 17C and D). While we do not know the actual southern extension of this region we recognize that it behaves as a microplate.

Cenozoic coastal block rotation changes are considered for the Paleogene extensional and Neogene compression stages of North Patagonia, in which case the presence of the North Patagonian Massif plays a key role in the regional tectonic evolution. This thick undeformable block, more rooted in the asthenosphere wedge than the surrounding back arc, is the support point for the deformation of the thinner back arc crust with respect to the thicker continental coast blocks (levers) as the plate margin changes from subduction to

transurrence (Figs. 15, 16 and 17). This allows the proposal of a new tectono-magmatic model: The coastal blocks of the northern Patagonia Andean segment break into two lever arms at the latitude of Loncoche. Each of the two lever arms has wheelbarrow lever geometry (rotation axis–load–effort) (Figs. 16 and 17). With this simple double lever system, the northern Patagonia Andean segment is subjected to extension in the regions North and South of the support point (NPM) following the partial rotation of the two segments. Accordingly, the calc-alkaline magmatism is shifted from the arc to the former back arc, as synextensional calc-alkaline magmatism interbedded with alkaline/tholeiitic lava flows. The origin of this synextensional bimodal magmatism is most likely to be a consequence of decompression melting of the enriched lithosphere left by the previous slab subduction stage. At the apex of extension, Oligocene–early Miocene basins are developed in the former fore arc, arc and back arc. The support point (NPM) does not suffer any deformation other than faulting and strong uplift.

The Miocene reinstatement of subduction by Nazca plate (Fig. 17 D) has the effect of inverting the sense of rotation of the northern and southern coastal blocks and changing the tectonic setting from extension to compression causing an upper Miocene tectonic reversal.

These Paleogene North Patagonian geologic relationships suggest a transform margin setting much like the Neogene tectono-magmatic history of western United States, with the transcurrent plate margin (jumping within the continental plate) at the San Andreas fault system (Atwater and Stock, 1998) and the synextensional bimodal volcanism with major ignimbrite flare up and basalts in the Basin and Range that represents the former back arc (Gans et al., 1989, Hawkesworth et al., 1995, Hooper et al., 1995), as the Colorado Plateau (undeformable block) is uplifted.

Acknowledgements

We are especially grateful to Michael O. Woodburne of the Department of Geology, of the Museum of Northern Arizona (Flagstaff) for his generous contributions, encouragement and help. We thank L. Dalla Salda for his thoughtful discussions and to Eduardo Suarez for his assistance with the figures. We are also in debt to two anonymous reviewers, whose comments substantially improved the manuscript. This work was supported with grants from projects of UNLP11N/534, CONICET PID 5080 and 00916, NSFDEB-0919071 of Peter Wilf, PRIN-COFIN 2007, and financial support to A. Castro (Grant: CGL2007-63237/BTE).

References

- Alic, V.I., Haller, M.I., Féraud, G., Bertrand, H., 2002. Volcanismo Alcalino Paleógeno en los alrededores de Paso de Indios. Provincia del Chubut. Actas del XV Congreso Geológico Argentino. El Calafate. Ponencia, p. 195.
- Aragón, E., Mazzoni, M.M., 1997. Geología y estratigrafía del complejo volcánico piroclástico del río Chubut medio (Eoceno), Chubut, Argentina. Revista de la Asociación Geológica Argentina 52 (3), 243–256.
- Aragón, E., Aguilera, Y., González, P., Gómez Peral, L., Cavarozzi, C.E., 2001. El Intrusivo Florentina del Complejo Volcánico Piroclástico del Río Chubut medio: un ejemplo de Etmolito o Embudo. Revista de la Asociación Geológica Argentina 56 (2), 161–172.
- Aragón, E., González, P., Aguilera, Y., Marquetti, C., Cavarozzi, C.E., Ribot, A., 2004a. El domo vitrofórico Escuela Piedra Parada del Complejo volcánico piroclástico del río Chubut Medio. Revista de la Asociación Geológica Argentina 59 (4), 607–618 Patagonia special paper.
- Aragón, E., Aguilera, Y., Consoli, V., Cavarozzi, C.E., Ribot, A., 2004b. Las Andesitas Estrechura del Complejo Volcánico Piroclástico del Río Chubut medio (Paleoceno-Eceno medio). Revista de la Asociación Geológica Argentina 59 (4), 619–633 Patagonia special paper.
- Aragón, E., Aguilera, Y., Cavarozzi, C., Ribot, A., 2005. Basaltos Alcalinos en el Complejo Volcánico-Piroclástico del Río Chubut medio. Actas XVI Congreso Geológico Argentino. Actas 1, 485–486.
- Aragón, E., Aguilera, Y., Cavarozzi, C.E., Ribot, A., 2010. The North Patagonian Altiplano and the Somon Cura basaltic plateau. Geociências 29 (4), 527–532 Sao Paulo, Brasil.
- Aragón, E., Castro, A., Díaz-Alvarado, J., Liu, D.-Y., in press. The north Patagonian batholith at Paso Puyehue (Argentina–Chile). SHRIMP ages and compositional features. Journal of South American Earth Sciences, pp 1–8.

- Atwater, T.M., Stock, J., 1998. Pacific–North America plate tectonics of the Neogene southwestern United States: an update. In: Ernst, W.G., Nelson, C.A. (Eds.), *The Clarence A. Hall, Jr. Volume. Geological Society of America*, pp. 393–420.
- Barazangi, M., Isacks, B.L., 1979. Subduction of Nazca plate beneath Peru: evidence from spatial distribution of earthquakes. *Geophysical Journal of the Royal Astronomical Society* 57, 537–555.
- Beck, M.E., 1988. Analysis of Late Jurassic–Recent paleomagnetic data from active plate margins of South America. *Journal of South American Earth Sciences* 1 (1), 39–52.
- Beck, M.E., Drake, R., Butler, R.F., 1986. Paleomagnetism of Cretaceous volcanic rocks from central Chile and implications for the tectonics of the Andes. *Geology* 14, 132–136.
- Beck, M.E., Burmester, R.F., Cembrano, J., Drake, R., García, A.R., Hervé, F., Munizaga, F., 2000. Paleomagnetism of the North Patagonian batholith, southern Chile. An exercise in shape analysis. *Tectonophysics* 326, 185–202.
- Bijwaard, H., Spakman, W., 2000. Non-linear global P-wave tomography by iterated linearized inversion. *Geophysical Journal International* 141, 71–82.
- Bijwaard, H., Spakman, W., Engdahl, E.R., 1998. Closing the gap between regional and global travel time tomography. *Journal of Geophysical Research* 103, 55–78.
- Cahill, T., Isacks, B.L., 1992. Seismicity and shape of the subducted Nazca plate. *Journal of Geophysical Research* 97, 17503–17529.
- Cande, S.C., Leslie, R.B., 1986. Late Cenozoic tectonics of the Southern Chile trench. *Journal of Geophysical Research* 91 (B1), 471–496.
- Cazau, L., Mancini, D., Cangini, J., Spallettil, L., 1989. Cuenca Ñirihuau. In: Chebli, G and Spalletti, L. (Eds): *Cuencas Sedimentarias de Argentina. Correlación Geológica* 6, 299–318.
- Charrier, R., Baeza, O., Elgueta, S., Flynn, J.J., Gans, P., Kay, S.M., Muñoz, N., Wyss, A.R., Zurita, E., 2002. Evidence for Cenozoic extensional basin development and tectonic inversion south of the flat-slab segment, southern Central Andes, Chile (33°–36°S. L.). *Journal of South American Earth Sciences* 15, 117–139.
- Cingolani, C., Hervé, F., Munizaga, F., Pankhurst, R.J., Parada, M.A., Rapela, C., 1991. The magmatic evolution of northern Patagonia: new impressions of pre-Andean and Andean Tectonics. *Geological Society of America Special Paper* 265, 29–44.
- Cingolani, C., Varela, R., Dalla Salda, L., Kawashita, K., 1993. Los granitoides del cerro Veladero, río de la Troya, provincia de La Rioja: estudio geocronológico e implicancias tectónicas. 12 Congreso Geológico Argentino y 2 Congreso de Exploración de Hidrocarburos: Actas, vol. 4, pp. 68–74. Mendoza.
- Coria, B.L., Nullo, F., Proserpio, C., Ramos, V.A., 1975. Tectónica de basamento de la región occidental del macizo norpatagónico. *Revista de la Asociación Geológica Argentina* 30 (4), 361–383.
- de Ignacio, C., López, I., Oyarzun, R., Márquez, A., 2001. The Northern Somuncura plateau basalts a product of slab-induced, shallow asthenospheric upwelling? *Terra Nova* 13 (2), 117–121.
- de Silva, S.L., 1991. Styles of zoning in central Andean ignimbrites: insights into magma chamber processes. *Geological Society of America Special Paper* 265, 217–232.
- Engdahl, E.R., Van der Hilst, R.D., Berrocal, J., 1995. Imaging subducted lithosphere beneath South America. *Geophysical Research Letters* 22 (16), 2317–2320.
- Engdahl, E.R., Van der Hilst, R.D., Buland, R., 1998. Global teleseismic earthquake relocation with improved travel times and procedures for depth determinations. *Bulletin of the Seismological Society of America* 88, 722–743.
- Forsythe, R., Nelson, E., 1985. Geological manifestation of ridge collision: evidence from the Golfo de Penas–Taitao Basin, Southern Chile. *Tectonics* 4 (5), 447–495.
- Gans, P.B., Mahood, G.A., Schermer, E., 1989. Synextensional magmatism in the Basin and Range Province; a case study from the eastern Great Basin. *Geological Society of America Special Paper* 233, 53.
- García, A.R., Beck, M.E., Burmester, R.F., Munizaga, F., Hervé, F., 1988. Paleomagnetic reconnaissance of the Los Lagos, Southern Chile, and its tectonic implications. *Revista Geológica de Chile* 15 (1), 13–30.
- Gerlach, D., Frey, F., Moreno, H., López-Escobar, L., 1988. Recent volcanism in the Puyehue–Cordón Caulle region, southern Andes, Chile (40.5°S): petrogenesis of evolved lavas. *Journal of Petrology* 29, 333–382.
- Giacosa, R., Heredia, N., 2004. Structure of the North Patagonian thick-skinned fold-and-thrust belt, southern central Andes, Argentina (41°–42° S). *Journal of South American Earth Sciences* 18, 61–72.
- Giacosa, R.E., Márquez, M.J., 1999. Jurásico y Cretácico de la Cordillera Patagónica Septentrional y Precordillera Patagónica. In: Caminos, R. (Ed.), *Geología Argentina*, vol. 29. Servicio Geológico Nacional, Buenos Aires, Anales, pp. 444–459.
- Gill, J.B., 1981. *Orogenic Andesites and Plate Tectonics*. Springer-Verlag, New York.
- González Díaz, E.F., 1982. Geocronological zonation of granitic plutonism in the northern Patagonian Andes of Argentina: the migration of intrusive cycles. *Earth Science Review* 18 (3–4), 365–393.
- González Díaz, E.F., Malagnino, E.C., 1984. Geomorfología de la Provincia de Río Negro. 9° Congreso Geológico Argentino. Relatorio, p. 159.
- Gosses, J., Carroll, A., Aragón, E., Singer, B., 2006. The Laguna del Huco Formation: lacustrine and sub-aerial caldera fill. Chubut Province, Argentina – GSA Abstract: October meeting.
- Gudmundsson, O., Sambridge, M., 1998. A Regionalized Upper Mantle (RUM) seismic model of the Earth. *Journal of Geophysical Research* B4, 7121–7136.
- Gutscher, M.A., Spakman, W., Bijwaard, H., Engdahl, E.R., 2000. Geodynamics of flat subduction: seismicity and tomographic constraints from the Andean arc region. *Tectonics* 19 (5), 814–833.
- Haschke, M., Günther, A., Melnick, D., Ehtler, H., Reutter, K.J., Scheuber, E., Oncken, O., 2006. Central and Southern Andean tectonic evolution inferred from arc magmatism. In: Oncken, O., Chong, G., Franz, G., Giese, P., Götze, H.J., Ramos, V.A., Strecker, M.R., Wigger, P. (Eds.), *The Andes Active Subduction Orogeny*. Springer, pp. 337–353.
- Hawkesworth, C., Turner, S., Gallagher, K., Hunter, A., Bradshaw, T., Rogers, N., 1995. Calc-alkaline magmatism, lithospheric thinning and extension in the Basin and Range. *Journal of Geophysical Research* 100 (B7), 10,271–10,286.
- Heintz, M., Debayle, E., Vauchez, A., 2005. Upper mantle structure of the South American continent and neighboring oceans from surface wave tomography. *Tectonophysics* 406, 115–139.
- Hervé, F., Faundez, V., Calderón, M., Massonne, H.J., Willner, A.P., 2007. Metamorphic and plutonic basement complexes. In: Moreno, T., Gibbons, E. (Eds.), *The Geology of Chile, Special, vol. GSL*, pp. 5–19.
- Hickey-Vargas, R., Frey, F.A., Gerlach, D.C., López-Escobar, L., 1986. Multiple sources for basaltic arc rocks from the Southern Volcanic Zone of the Andes (34°–41S): trace element and isotopic evidence for contributions from subducted oceanic crust, mantle and continental crust. *Journal of Geophysical Research* 91 (6), 5963–5983.
- Hickey-Vargas, R., Moreno, H., López-Escobar, L., Frey, F.A., 1989. Geochemical variations in Andean basaltic and silicic lavas from the Villarrica–Lanin volcanic chain (39.5°S): an evaluation of source heterogeneity, fractional crystallization and crustal assimilation. *Contributions to Mineralogy and Petrology* 103, 361–386.
- Hooper, P.R., Bailey, D.G., McCarley Holder, G.A., 1995. Tertiary calc-alkaline magmatism associated with lithosphere extension in the Pacific Northwest. *Journal of Geophysical Research* 100 (B7), 10,303–10,319.
- Hyndman, R.D., Currie, C.A., Mazzotti, S.P., 2005. Subduction zone back arcs, mobile belts, and orogenic heat. *GSA Today* 15, 4–10.
- Jordan, T.E., Matthew, Burns W., Veiga, R., Pángaro, F., Copeland, P., Kelley, S., Mpodozis, C., 2001. Extension and basin formation in the southern Andes caused by increased convergence rate: a mid-Cenozoic trigger for the Andes. *Tectonics* 20 (3), 308–324.
- Kay, S.M., Rapela, C.W., 1987. El volcanismo del Terciario inferior y medio en los Andes Norpatagónicos (40°–42° 30'S): Origen de los magmas y su relación con variaciones en la oblicuidad de la zona de subducción. 10° Congreso Geológico Argentino. Actas 4, 192–194.
- Kay, S.M., Ardolino, A.A., Franchi, M., Ramos, V., 1993. Origen de la meseta de Somon Cura: distribución y geoquímica de sus rocas volcánicas máficas. XII° Congreso Geológico Argentino, Actas, vol. 4, pp. 236–248.
- Kay, S.M., Gorring, M., Ramos, V., 2004. Magmatic sources, setting and causes of Eocene to Recent Patagonian plateau magmatism (36°S to 52°S). *Revista de la Asociación Geológica Argentina* 59 (4), 556–568.
- Lonsdale, P., 2005. Creation of the Cocos and Nazca plates by fission of the Farallon plate. *Tectonophysics* 404, 237–264.
- López-Escobar, L., Frey, F.A., Vergara, M., 1976. Andesites from central-south Chile: trace elements abundances and Petrogenesis. In: González-Ferrán, O. (Ed.), *International Association of Volcanology and Geochemistry of the Earth's Interior*, pp. 725–761.
- López Escobar, L., Frey, F.A., Vergara, M., 1977. Andesites and high alumina basalts from the central-south high Chilean Andes: geochemical evidence bearing on their petrogenesis. *Contributions to Mineralogy and Petrology* 63, 199–228.
- López-Escobar, L., Parada, M.A., Moreno, H., Frey, F.A., Hickey-Vargas, R.L., 1992. A contribution to the petrogenesis of Osorno and Calbuco volcanoes, Southern Andes (41°00'–41°30'S): comparative study. *Revista Geológica de Chile* 19 (2), 211–226.
- López-Escobar, L., Kilian, R., Kempton, P., Tagiri, M., 1993. Petrography and geochemistry of Quaternary rocks from the Southern Volcanic Zone between 41°30' and 46°00'S, Chile. *Revista Geológica de Chile* 20 (1), 35–55.
- López-Escobar, L., Cembrano, J., Moreno, H., 1995. Geochemistry and tectonics of the Chilean Southern Andes basaltic Quaternary volcanism (37°–46°S). *Revista Geológica de Chile* 22 (2), 219–234.
- MacDonald, G.A., 1968. Composition and origin of Hawaiian lavas. In: Cotas, R.R., Hay, R.L., and Anderson, C.A. (eds.), *Studies in volcanology: a memoir in honour of Howel Williams*. Geological Society of America 116, 477–522.
- Mancini, C.D., Serna, M.J., 1989. Evaluación petrolera de la cuenca de Ñirihuau, Sudoeste de la Argentina. I Congreso Nacional de Hidrocarburos, vol. 2, pp. 739–762.
- Mazzoni, M.M., Kawashita, K., Harrison, S., Aragón, E., 1991. Edades radiométricas Eocenas en el borde Occidental del Macizo Norpatagónico. *Revista de la Asociación Geológica Argentina* 46 (1–2), 150–158.
- Mella, M., Muñoz, J., Vergara, M., Klohn, E., Farmer, L., Stern, C.R., 2005. Petrogenesis of Pleistocene Tronador Volcanic Group, Andean Southern Volcanic Zone. *Revista Geológica de Chile* 32 (1), 132–154.
- Miyashiro, A., 1974. *Metamorphism and Metamorphic Belts*. Allen and Unwin, Winchester, Mass. 492 pp.
- Munizaga, F., Hervé, F., Drake, R., Pankhurst, R., Brook, M., Snelling, N., 1988. Geochronology of the granitoids of the Andean lake region 39°–42° Lat. South central Chile, preliminary results. *Journal of South American Earth Sciences* 1, 309–316.
- Muñoz, J., Troncoso, R., Duhart, P., Crignola, P., Farmer, L., Stern, C.R., 2000. The Mid-Tertiary coastal magmatic belt in south-central Chile (36°–43°S): its relation to crustal extension, mantle upwelling, and the late Oligocene increase in the rate of oceanic plate subduction beneath South America. *Revista Geológica de Chile* 27 (2), 177–203.
- Pankhurst, R.J., Weaver, S.D., Hervé, F., Larrondo, P., 1999. Mesozoic–Cenozoic evolution of the North Patagonian Batholith in Aysén, Southern Chile. *Journal of the Geological Society, London* 156, 673–694.
- Pardo, Casas F., Molnar, P., 1987. Relative motion of the Nazca (Farallon) and South American plates since late Cretaceous time. *Tectonics* 6 (3), 233–248.
- Pearce, J.A., Harris, N.B.W., Tindle, A.G., 1984. Trace element discrimination diagrams for the tectonic interpretation of granitic rocks. *Journal of Petrology* 25, 956–983.
- Rapela, C.W., 1987. El Batolito Patagónico entre 40°30' y 41°15'S; Estudio Geoquímica preliminar. Actas del X Congreso Geológica Argentino, Tucumán, Argentina, vol. 4, pp. 21–23.
- Rapela, C.W., Kay, S.M., 1988. Late Paleozoic to Recent magmatic evolution of Northern Patagonia. *Episodes* 11 (3), 176–182.
- Rapela, C.W., Spalletti, L., Merodio, J.C., 1983. Evolución magmática y geotectónica de la Serie Andesítica andina (Paleoceno–Eoceno) en la cordillera norpatagónica. *Revista de la Asociación Geológica Argentina* 38 (3–4), 469–484.

- Rapela, C.W., Spalletti, L., Merodio, J.C., Aragón, E., 1987. Temporal evolution and spatial variation of the lower Tertiary Andean volcanism (40–42°S). *Journal of South American Earth Sciences* 1, 1–14.
- Rojas, C., Beck, M.E., Burmester, R.F., Cembrano, J., Hervé, F., 1994. Paleomagnetism of the mid-Tertiary Ayacara Formation, southern Chile: counter clockwise rotation in a dextral shear zone. *Journal of South American Earth Sciences* 7 (1), 45–56.
- Silvestro, J., Zubiri, M., 2008. Convergencia oblicua: Modelo estructural alternativo para la dorsal Neuquina (39°S)- Neuquén. *Revista de la Asociación Geológica Argentina* 63 (1), 49–64.
- Somoza, R., 1998. Updated Nazca (Farallón)–South America relative motions during the last 40 Ma: implications for mountain building in the central Andean region. *Journal of South American Earth Sciences* 11, 211–215.
- Somoza, R., Ghidella, M.E., 2005. Convergencia en el margen occidental de América del Sur durante el Cenozoico: subducción de las placas de Nazca, Farallón y Aluk. *Revista de la Asociación Geológica Argentina* 60 (4), 797–809.
- Spalletti, L.A., 1983. Paleogeografía de la Formación Ñirihua y sus equivalentes en la región occidental de Neuquén, Río Negro y Chubut. *Revista de la Asociación Geológica Argentina* 38 (3–4), 454–468.
- Stern, C.R., 1991. Role of subduction erosion in the generation of the Andean magmas. *Geology* 19, 78–81.
- Tassara, A., Yáñez, G., 2003. Relación entre el espesor elástico de la litosfera y la segmentación tectónica del margen Andino (15°–47°). *Revista Geológica de Chile* 30 (2), 159–186.
- Tormey, D.R., Hykey-Vargas, R., Frey, F.A., López Escobar, L., 1991. Recent lavas from the Andean volcanic front (33 to 42°S); interpretations of along-arc compositional variations. *Geological Society of America Special Paper* 265, 57–77.
- Vietor, T., Echtler, H., 2006. Episodic Neogene southward growth of the Andean subduction orogen between 30°S and 40°S – plate motions, mantle flow, climate, and upper-plate structure. In: Oncken, O., Chong, G., Franz, G., Giese, P., Götze, H.J., Ramos, V.A., Strecker, M.R., Wigger, P. (Eds.), *The Andes Active Subduction Orogeny*. Springer, pp. 375–400.
- Vietor, T., Echtler, H., Müller, H., Oncken, O., Ladage, S., 2004. Late Miocene block rotations in the South Chilean offshore forearc (38,5°S) linked to backarc shortening; paleomagnetic and bathimetric evidences. EOS85(47) Fall Meeting Supplements (Abstract).
- Walker, J.A., Moulds, T.N., Zentilli, M., Feigenson, M.D., 1991. Spatial and temporal variations in volcanics of the Andean Central Volcanic Zone (26 to 28°S). *Geological Society of America Special Paper* 265, 139–155.
- Wilf, P., Johnson, R.K., Cúneo, R.N., Smith, M.E., Singer, B.S., Gandolfo, M.A., 2005. Eocene plant diversity at Laguna del Hunco and Río Pichileufu, Patagonia, Argentina. *The American Naturalist* 165 (6), 634–650.
- Wood, D.A., 1980. The application of a Th–Hf–Ta diagram to problems of tectonomagmatic classification and to establish the nature of crustal contamination of basic lavas of the British Tertiary Volcanic Province. *Earth and Planetary Scientific Letters* 50, 11–30.
- Yáñez, G., Cembrano, J., Pardo, M., Ranero, C., Selles, D., 2002. The Challenger–Juan Fernández–Maipo major tectonic transition of the Nazca–Andean subduction system at 33–34°S: geodynamic evidence and implications. *Journal of South American Earth Sciences* 15, 23–38.